Graphical Abstract

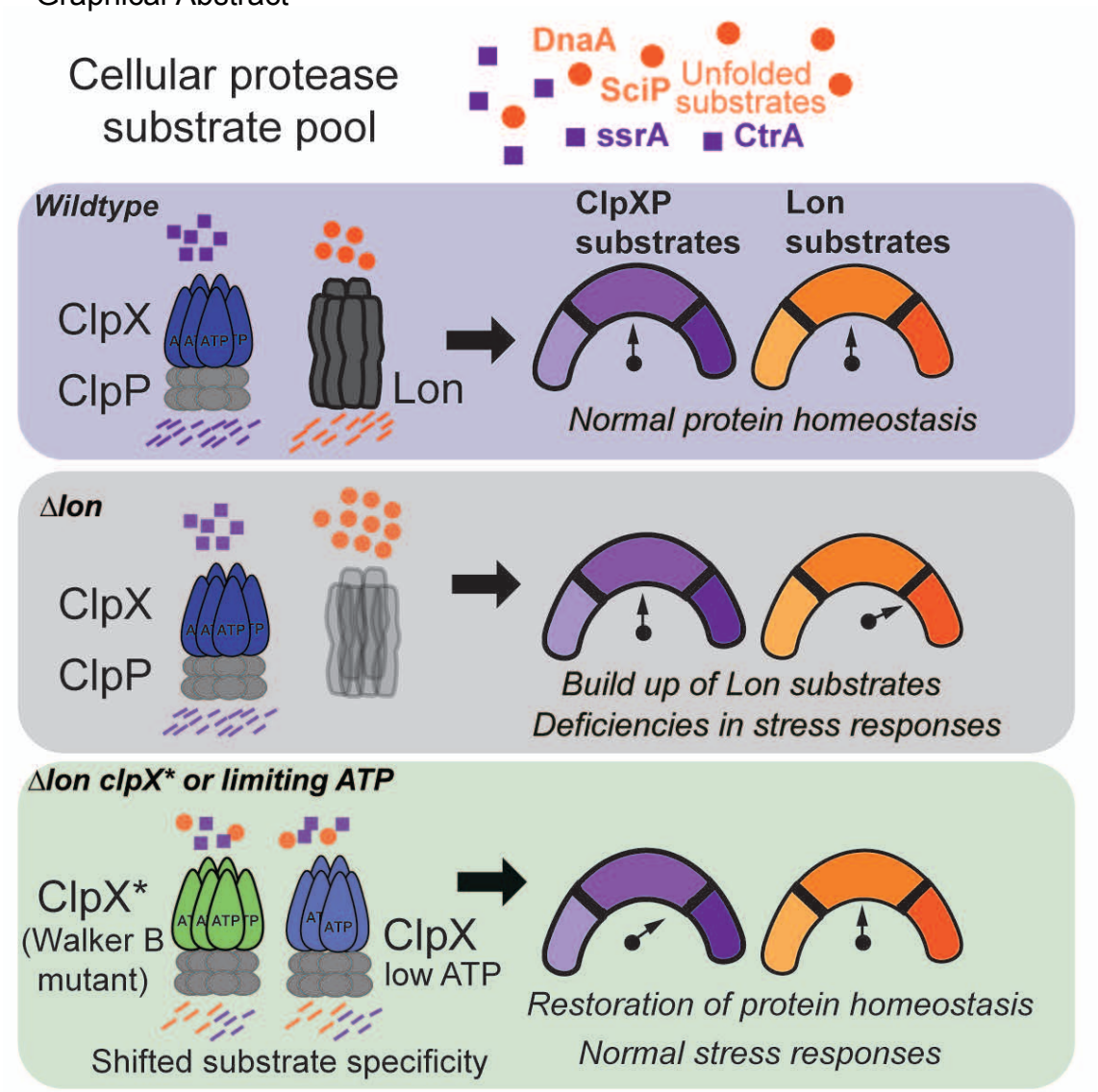

eTOC

AAA+ proteases, such as Lon and ClpXP, select distinct targets for degradation to maintain proteostasis. Mahmoud et al. show that ATP hydrolysis can tune substrate specificity of ClpX, allowing ClpX to degrade Lon-restricted substrates under limiting ATP conditions or in the presence of a ClpX mutant.

Highlights

- A Walker B mutation of the AAA+ protease ClpX alters substrate specificity
- ClpX mutant degrades new substrates but degrades canonical substrates less well
- Decreasing ATP levels enhances ClpXP mediated degradation of some classes of substrates
- ATP-induced changes in conformational states accompany alterations in ClpX specificity

ATP hydrolysis tunes specificity of a AAA+ protease

Samar A. Mahmoud[1,2], Berent Aldikacti[1,2], Peter Chien[1,2*]

Affiliations:

[1]Department of Biochemistry and Molecular Biology, [2]Molecular and Cellular Biology Program, University of Massachusetts Amherst, Amherst, MA 01003, USA.

***Corresponding Author:**

Peter Chien (Lead contact)
240 Thatcher Rd, Amherst, MA 01003
pchien@umass.edu
(413) 545-2310

Summary

In bacteria, AAA+ proteases such as Lon and ClpXP degrade substrates with exquisite specificity. These machines capture the energy of ATP hydrolysis to power unfolding and degradation of target substrates. Here, we show that a mutation in the ATP binding site of ClpX shifts protease specificity to promote degradation of normally Lon-restricted substrates. However, this ClpX mutant is worse at degrading ClpXP targets, suggesting an optimal balance in substrate preference for a given protease that is surprisingly easy to alter. *In vitro*, wildtype ClpXP also degrades Lon-restricted substrates more readily when ATP levels are reduced, similar to the shifted specificity of mutant ClpXP, which has altered ATP hydrolysis kinetics. Based on these results, we suggest that rates of ATP hydrolysis not only power substrate unfolding and degradation, but also tune protease specificity. We consider various models for this effect based on emerging structures of AAA+ machines showing conformationally distinct states.

Introduction

Energy-dependent protein degradation regulates normal growth and stress responses in all cells. In bacteria, regulated proteolysis is carried out by several energy-dependent AAA+ (ATPases associated with cellular activities) proteases which include Lon, ClpXP, ClpAP, HslUV, FtsH (Gur et al., 2011; Mahmoud and Chien, 2018). These proteases share a similar general architecture containing an unfoldase domain and a non-specific peptidase (Sauer and Baker, 2011). The two domains can be encoded on a single polypeptide, such as in the case of Lon and FtsH, or they can be encoded by separate proteins, an ATPase, such as ClpX, and a peptidase, such as ClpP (Baker and Sauer, 2012; Langklotz et al., 2012; Lee and Suzuki, 2008). Using the power of ATP hydrolysis, the unfoldase recognizes, unfolds, and translocates substrates into the sequestered peptidase chamber to be degraded. Because they are critical for maintaining proteostasis, loss of these proteases results in defects in growth, cell-cycle progression, stress responses, and pathogenesis (Breidenstein et al., 2012; Howard-Flanders et al., 1964; Jenal and Fuchs, 1998; Rogers et al., 2016).

64

65 Despite the similarities in both architecture and mechanism, these proteases generally
66 have distinct niches of substrate preference. For example, in *Caulobacter crescentus*,
67 Lon is the principal protease for degradation of the replication initiator DnaA (Jonas et
68 al., 2013), the methyltransferase CcrM (Wright et al., 1996), and the transcriptional
69 regulator SciP (Gora et al., 2013). By contrast, the ClpXP protease degrades cell-cycle
70 factors like CtrA and TacA during cell-cycle progression through an adaptor hierarchy
71 (Joshi et al., 2015). Lon is also responsible for misfolded protein degradation
72 (Goldberg, 1972; Gur and Sauer, 2008; Jonas et al., 2013). However, while a handful of
73 target substrates for these AAA+ proteases have been identified, it remains unclear how
74 proteases are able to discriminate among protein targets and recognize distinct
75 substrates for irreversible degradation.
76

77 In this work, we find that a variant of ClpX (*clpX**) can compensate for the absence of
78 the Lon protease. Expression of *clpX** suppresses defects in motility, growth,
79 filamentation, and sensitivity to stress normally seen in a Δ*lon* strain. In addition to this
80 phenotypic rescue, degradation of normal Lon substrates is restored *in vivo* and *in vitro*
81 by ClpX*P. This increased ability to degrade noncanonical substrates comes at the cost
82 of reduced degradation of ClpXP-specific substrates, resulting in fitness defects in
83 otherwise wildtype strains expressing the *clpX** allele. Further mechanistic
84 characterization shows that ClpX* has reduced catalytic efficiency for ATP hydrolysis,
85 suggesting a connection between ATP utilization and substrate specificity. Consistent
86 with this, limiting ATP for wildtype ClpXP shifts substrate preferences similar to that of
87 ClpX*P. Limited proteolysis, differential scanning fluorimetry (DSF), and hydrogen-
88 deuterium exchange mass spectrometry (HDX-MS) show that the ClpX unfoldase
89 adopts distinct conformations under these ATP limiting or saturating conditions. Taken
90 together, our work demonstrates that ATP-dependent dynamics between
91 conformational states are important for substrate recognition by AAA+ unfoldases.
92

93 **Results**

94 **A suppressor screen identifies a *clpX* mutant which rescues *Δlon***

95 We reasoned that a suppressor screen would allow us to identify Lon-related
96 interactions and used a transposon library to identify mutations that restore motility to a
97 *Δlon* strain. We isolated a high motility mutant with a transposon insertion in
98 CCNA_00264; however, transduction experiments revealed that this transposon alone
99 was not able to rescue motility (Figure S1A). Sequencing the genome of the suppressor
100 strain showed a point mutation in *clpX*, which resulted in a single amino acid change
101 from glycine 178 to alanine (*clpX**). This glycine is highly conserved among ClpX
102 homologs and immediately adjacent to the Walker B motif (Figure S1C). By generating
103 the *clpX** allele in a *Δlon* background, we found that *clpX** on its own partially restores
104 motility (Figure 1A).
105
106 We were intrigued that a single mutation in *clpX* could restore motility to cells lacking
107 Lon and chose to further characterize this strain. Cells lacking Lon show growth defects
108 that exhibit as an extended lag phase and reduced cell mass accumulation in stationary
109 phase (Figure 1A). The *clpX** allele rescues the mass accumulation defect, but not the
110 extended lag (Figure 1A). *Δlon* strains also have significant morphological deficiencies
111 including elongated cell length and longer stalks, external polar organelles characteristic
112 of *Caulobacter*. We found that the *clpX** mutant restored the cell length of Δ*lon* strains to
113 near wildtype levels (Figure 1B, 1C). However, stalks remained elongated in the *Δlon*
114 *clpX** strain (Figure 1B, 1C).
115
116 We next wondered if, in addition to suppression of *Δlon* morphological and growth
117 defects, sensitivity to certain stressors would be suppressed by this *clpX** allele. One of
118 the originally described phenotypes for *E. coli lon* mutants is DNA damage sensitivity
119 (Mizusawa and Gottesman, 1983; Witkin, 1946) and *Caulobacter ⊿lon* strains are also
120 highly sensitive to various DNA damaging agents (Zeinert et al., 2018), including
121 mitomycin C (MMC) (Figure 1C). We found that Δ*lon clpX** was 100-fold more resistant
122 to MMC than *Δlon* alone (Figure 1C).
123
124 As mentioned previously, Lon is the major protease responsible for the degradation of
125 the replication initiator DnaA and *Δlon* strains accumulate excess chromosome content

126 (Jonas et al., 2013; Wright et al., 1996). Like the morphological abnormalities, over-
127 replication is suppressed in the Δ*lon clpX** strain which shows similar chromosome
128 content as wildtype cells (Figure 1D, S1D). To determine if this rescue extended to a
129 systems-level correction, we compared RNA-seq profiles of wildtype, Δ*lon* and Δ*lon*
130 *clpX** strains. As expected, many genes (435) are differentially expressed upon loss of
131 Lon (Figure 1E, Supplementary File 1), while the Δ*lon clpX** strain shows fewer
132 differences (119) with only 85 genes overlapping between these sets. Finally, we
133 assayed the overall physiological consequence of ClpX* using competitive fitness in
134 mixed cultures. We grew cultures of Δ*lon* or the Δ*lon clpX** strain together with Δ*lon*
135 strains constitutively expressing the Venus fluorescent protein (Persat et al., 2014). We
136 found that Δ*lon clpX** cells were more fit than Δ*lon* cells (Figure S1E). Our interpretation
137 is that expression of *clpX** in a Δ*lon* background largely shifts the phenotypes and
138 transcriptional landscape to more wildtype profiles.
139
140 **ClpX* restores degradation of Lon substrates *in vivo***
141 Because cells lacking Lon would accumulate normally degraded substrates, we
142 hypothesized that the rescue we observed in the *Δlon clpX** strain was likely due to
143 lower levels of Lon substrates, such as DnaA, CcrM, and SciP (Figure 2A) (Wright et al.,
144 1996; Gora et al., 2013; Jonas et al., 2013). As expected, in unsynchronized cells,
145 DnaA and CcrM levels are higher in the Δ*lon* strain than in wildtype (Figure 2B).
146 Similarly, SciP levels are higher in Δ*lon* swarmer cells in comparison to wildtype (Figure
147 2D). Interestingly, levels of DnaA and SciP are restored to wildtype levels in the Δ*lon*
148 *clpX** strain; however, CcrM remained at higher levels (Figure 2B). The reduced levels
149 of DnaA likely explain the rescue of replication defects and enrichment analysis of the
150 RNA-seq results shows that the SciP-controlled regulon and cell-cycle gene expression
151 are largely restored in the Δ*lon clpX** strain (Figure S2). We reasoned that expression
152 of *clpX** rescues normal growth and critical stress responses in a Δ*lon* strain through
153 restoring wildtype levels of key proteins.
154
155 Next, we explored the mechanism by which a mutation in ClpX restores steady state
156 levels of DnaA and SciP. Because DnaA and SciP are controlled by proteolysis, we

157 suspected that protein turnover may be affected. As expected, DnaA is largely
158 stabilized in Δ*lon* strains (Figure 2C; Jonas, et al. 2013); however, we found that DnaA
159 degradation was restored in the Δ*lon clpX* strain*, with a half-life similar to that of
160 wildtype (Figure 2D). SciP protein dynamics and cell-cycle phase specific levels were
161 also restored in Δ*lon clpX** cells (Figure 2D). By contrast, CcrM degradation was still
162 solely dependent on Lon, even when *clpX** was present, in both unsynchronized cells
163 (Figure 2C) and during cell-cycle progression (Figure S2D).
164
165 We considered that changes in protein turnover could be either due to a gain-of-function
166 in the *clpX** mutant or by indirect cellular effects associated with a loss-of-function in
167 *clpX*. To test this, we created a merodiploid *Δlon* strain expressing a second copy of
168 *clpX* or *clpX** under control of the native promoter along with a normal chromosomal
169 copy of *clpX*. We reasoned that if the effect was direct, then expression of *clpX** would
170 be sufficient to restore DnaA degradation. If the effect was indirect, then DnaA would
171 remain stable. Consistent with a gain-of-function phenotype for the *clpX** allele, we
172 found that DnaA turnover increased upon expression of *clpX** but not wildtype *clpX*
173 (Figure 2E). Similarly, the phenotypic rescue we observed in the *Δlon clpX** strain was
174 also due to a gain-of-function activity as the merodiploid strain expressing *clpX**
175 suppressed *Δlon* defects, such as growth, motility, and genotoxic stress tolerance
176 (Figure S2E-G). Because ClpXP is a AAA+ protease, we hypothesized that ClpX*P (the
177 protease complex of the variant ClpX* with wildtype ClpP) was now able to recognize
178 and degrade substrates normally degraded by Lon.
179
180 **ClpX*P directly degrades Lon substrates *in vitro***
181 As a direct test of our hypothesis, we purified the ClpX* variant and reconstituted
182 degradation *in vitro*. Upon initial characterization of purified ClpX*, we found that it
183 formed an active ATPase, but hydrolyzed ATP three times faster than wildtype (Figure
184 S3A). Consistent with the fact that Lon is the principal protease for DnaA degradation
185 (Jonas et al., 2013; Liu et al., 2016), we found that wildtype ClpXP poorly degraded
186 DnaA *in vitro* (Figure 3A). However, purified ClpX*P could degrade DnaA four-fold
187 faster than ClpXP (Figure 3A). Similarly, SciP was degraded three-fold faster by ClpX*P

188 in comparison to ClpXP (Figure 3A). Finally, as predicted from our *in vivo* results, CcrM
189 was not degraded by either ClpX*P or ClpXP (Figure 3A, Figure S3B), but was well
190 degraded by Lon (Figure S3B). Thus, ClpX* appears to have an expanded substrate
191 profile which includes some Lon substrates, but others, such as CcrM, remain exclusive
192 to Lon.
193
194 Lon recognizes exposed hydrophobic amino acids (Gur and Sauer, 2008) and is best
195 known as a quality control protease that eliminates mis/unfolded proteins (Goff et al.,
196 1984). Given its altered specificity, we considered if ClpX* could now recognize these
197 substrates. Casein is commonly used as an *in vitro* model substrate for mis/unfolded
198 proteins. Lon robustly degrades fluorescently labeled casein, whereas wildtype ClpXP
199 poorly degrades this substrate (Figure 3B). Intriguingly, ClpX*P degrades FITC-casein
200 more than twice as fast as ClpXP (Figure 3B, Figure S3C). Similar to casein, ClpX*P
201 degrades another unfolded Lon substrate, a chemically denatured domain of titin tagged
202 with the hydrophobic sequence β20 (Gur and Sauer, 2008), better than wildtype ClpXP
203 (Figure S3D).
204
205 Because cells lacking Lon are sensitive to proteotoxic stresses that create misfolded
206 proteins and because ClpX*P is better at degrading mis/unfolded substrates than
207 wildtype ClpXP, we wondered if the Δ*lon clpX** strain would be more resistant to
208 stressors that induce cellular protein misfolding. Indeed, the presence of the *clpX** allele
209 protected Δ*lon* cells from hypersensitivity to the proteotoxic amino acid L-canavanine
210 (Figure 3B). We conclude that ClpX* has an altered substrate preference, which
211 includes DnaA, SciP, and unfolded proteins, whose degradation are normally governed
212 by the Lon protease.
213
214 **ClpX*P is deficient in degradation of native ClpXP substrates**
215 Mutations in ClpX that improve recognition of some substrates can have negative
216 consequences on others (Farrell et al., 2007). GFP-ssrA is a well-characterized ClpXP
217 substrate that is directly bound by the pore loops of ClpX (Fei et al., 2020; Gottesman et
218 al., 1998). We purified GFP fused to the *Caulobacter* ssrA tag (Chien, et al. 2007),

219 determined degradation rates by ClpX*P and ClpXP, and fit these rates to the
220 Michaelis-Menten equation. We found that ClpX*P degrades GFP-ssrA more poorly
221 than wildtype ClpXP, principally lowering the turnover rate (Figure 4A, Figure S4A),
222 suggesting that either ClpX* fails to irreversibly initiate degradation via the ssrA tag as
223 readily or is unable to translocate the reporter protein as well as wildtype ClpX.
224
225 CtrA is a master regulator in *Caulobacter* that inhibits replication initiation and regulates
226 the transcription of many cell-cycle genes (Laub et al., 2002; Wortinger et al., 2000). *In*
227 *vivo*, CtrA is degraded during the G1-S transition by ClpXP through the use of an
228 adaptor hierarchy (Domian et al., 1999; Jenal and Fuchs, 1998; Joshi et al., 2015; Quon
229 et al., 1996); however, *in vitro* CtrA can also be directly recognized by ClpXP as its C-
230 terminus resembles the ssrA tag (Chien et al., 2007). Consistent with a reduced ability
231 to recognize ClpXP substrates, ClpX*P degrades isolated CtrA more poorly than
232 wildtype (Figure 4B) and also shows reduced degradation of a CtrA-derived GFP
233 reporter (Smith et al., 2014) in the presence of the full adaptor hierarchy (Figure S4B).
234 We conclude that ClpX*P overall has a diminished ability to recognize and degrade
235 native substrates normally degraded by ClpXP.
236
237 **Deficiencies of ClpX* revealed when Lon is present**
238 The prior *in vitro* data suggests that rather than just expanding specificity, this mutation
239 has allowed ClpX*P to degrade Lon-dependent substrates better but at the cost of
240 degrading ClpXP-dependent ones. If this is true, while *clpX** is beneficial in a *Δlon*
241 background, we reasoned that it may be detrimental to *lon*$^+$ cells.
242
243 To test this hypothesis, we generated an otherwise wildtype strain with *clpX** as its sole
244 copy. We first examined ssrA tag turnover in this strain by using an ssrA derivative that
245 relies on the SspB adaptor for degradation (eGFP-ssrA(DAS)) (Chowdhury et al., 2010)
246 so that degradation would be sufficiently slowed to be visualized by western blotting.
247 Consistent with our *in vitro* experiments, we observed stabilization and dramatically
248 higher levels of eGFP-ssrA (DAS) in the *clpX** strain in comparison to wildtype (Figure
249 4C). We observed reduced CtrA degradation in the *clpX** strain, consistent with our *in*

250 *vitro* observations (Figure 4C). Finally, DnaA degradation is accelerated in the *clpX**
251 strains compared to wildtype – consistent with our findings that both Lon and ClpX*P
252 are able to degrade DnaA (Figures 4C).
253
254 To assess the overall impact of ClpX* on wildtype cells, we performed competition
255 assays as described previously using a wildtype strain constitutively expressing the
256 Venus fluorescent protein (Persat et al., 2014). We found that while nonfluorescent
257 wildtype cells could slightly outcompete the constitutive Venus expressing cells, the
258 *clpX** strain showed a substantial competitive disadvantage (Figure 4D). We also tested
259 for stress tolerances and found that *clpX** strains fail to survive genotoxic stress as
260 robustly as wildtype (Figure 4E). Our conclusion is that reduced fitness of the wildtype
261 *clpX** strain is likely due to reduced degradation of normal ClpXP substrates (such as
262 CtrA) and prolific degradation of normal Lon substrates (such as DnaA) that together
263 reduce overall fitness. Collectively, this supports our understanding that AAA+
264 proteases have been optimized for specific priorities in a cell – expansion of their
265 substrate profile, as seen with *clpX*,* can compensate for loss of other proteases, but at
266 the cost of their ability to recognize their normal substrates.
267
268 **Limiting ATP alters wildtype ClpXP substrate specificity**
269 To understand how this mutation in ClpX leads to enhanced degradation of certain
270 substrates, we further characterized the ATPase activity of ClpX*. While ClpX*
271 hydrolyzes ATP three-fold faster than wildtype ClpX at saturating ATP concentrations
272 (Figure S4A), Michaelis-Menten experiments showed that the K_M increases by 5-6 fold
273 and the k_{cat} for ATP hydrolysis increases by approximately 3 fold (Figure 5A). While K_M
274 does depend on k_{cat}, the magnitude of K_M increase given the change in k_{cat} suggests
275 that there may also be deficiencies in nucleotide binding of ClpX*. To test this, we used
276 ATP to compete off mant-ADP, a fluorescent ADP analog and we observed at least a
277 three-fold increase in the IC_{50} for ClpX*, suggesting that it binds ATP worse than
278 wildtype ClpX (Figure S5A). To make sure that the observed difference in the IC_{50}
279 between ClpX and ClpX* was due to changes in nucleotide binding and not because of
280 the hydrolysis of ATP in the assay, we also competed mant-ADP using ATPγS and

281 assayed changes using fluorescence polarization. Consistent with the ATP titration
282 described above, we calculated a higher IC_{50} for ATPγS for ClpX* (Figure S5B).
283
284 As seen previously, degradation of GFP-ssrA by ClpXP is precipitously lost below a
285 minimum threshold of ATP (Martin et al., 2008), with the ClpX*P threshold being higher
286 than that of wildtype, consistent with the higher K_M for ATP described above (Figure
287 S5C). For ClpX*P, casein degradation reduced monotonically as ATP concentration
288 was lowered (Figure 5B). In striking contrast, we found that for wildtype ClpXP, casein
289 degradation was increased at intermediate nucleotide concentrations compared to
290 saturating ATP (Figure 5B). Kinetic analysis shows that at these lower ATP
291 concentrations ClpXP degrades casein with a lower K_M and a similar V_{max} compared to
292 saturating ATP conditions (Figure 5C). Since $K_M = K_D + k_{cat}/k_{on}$, the lower K_M suggests
293 that, at a minimum, casein must bind better to ClpX at these concentrations.
294
295 These results suggest that ClpX specificity depends on ATP concentration and rates of
296 hydrolysis, with lower levels of ATP facilitating ClpX recognition of some substrates
297 better than at saturating ATP concentrations. Similar to casein, we saw this same
298 dependence *in vitro* with the Lon substrates DnaA and SciP (Figure 5D and S5D). To
299 test this effect *in vivo*, we monitored degradation of DnaA during starvation, which
300 should decrease cellular ATP levels, using a Δ*lon* Δ*clpA* strain to eliminate any non-
301 ClpX dependent degradation (Liu et al., 2016). We verified that glucose starvation
302 results in DnaA degradation in wildtype cells (Gorbatyuk and Marczynski, 2005; Figure
303 5E) and showed that starving Δ*lon* Δ*clpA* also markedly increased DnaA degradation
304 (Figure 5E). During this starvation there was also a drop in bulk ATP levels (Figure
305 S5E), though we note that the magnitude of the drop is less than the changes we
306 observe *in vitro* that alter ClpX specificity. We conclude that ClpX preference depends
307 on ATP binding or hydrolysis, with its specificity expanded under limiting ATP
308 conditions.
309
310 We considered if conformational changes in ClpX might explain the altered specificity of
311 wildtype ClpX at low ATP or the changes associated with ClpX*. Using limited

312 proteolysis to probe conformational differences we found that ClpX at low ATP was
313 more protease accessible than at high ATP (Figure 6A). Similarly, protease accessibility
314 of ClpX* at high ATP resembled the wildtype ClpX at low ATP (Figure 6A). Using
315 differential scanning fluorimetry (DSF), we found that ClpX* was destabilized in
316 comparison to wildtype ClpX at high ATP (Figure 6B). As expected, limiting ATP for
317 wildtype ClpX also resulted in less thermal stability (Figure 6B) as ATP binding is known
318 to be needed for ClpX oligomerization (Hersch *et al.*, 2005). Taken together, these
319 results suggest that under high ATP concentrations, the mutant ClpX* adopts a set of
320 conformational states that is overall less stable that wildtype.
321
322 To gain more clarity on what structural features might be different in these states, we
323 performed hydrogen-deuterium exchange coupled with mass spectrometry (HDX-MS) to
324 determine specific regions of ClpX and ClpX* that differ in dynamics. We compared
325 ClpX and ClpX* in high ATP conditions (4 mM) and found that ClpX* peptides generally
326 showed faster exchange than the equivalent peptides from wildtype ClpX (Figure 6C,
327 S6B-C). One of these peptides (residues 186-200) was the most deprotected in ClpX*
328 compared to ClpX and is buried in the pore of the closed substrate-bound structure of
329 ClpX (Protein Data Bank ID: 6PO1) (Figure 6C, Figure S6C). Speculation on these
330 results is discussed below.
331
332 **Discussion**
333 Because proteolysis is irreversible, degradation of substrates must be carefully
334 monitored to avoid toxic consequences. In bacteria, different energy dependent
335 proteases have distinct substrate preferences that allows them to collectively regulate
336 proteome dynamics. However, how these energy-dependent proteases choose their
337 target substrates from a pool of cellular proteins remains poorly understood. Certain
338 determinants that dictate specificity include degrons, or degradation tags, such as the
339 ssrA tag which marks proteins for degradation by ClpXP or ClpAP (Keiler, 2015; Keiler
340 et al., 1996). Specificity can be augmented through adaptor proteins that help deliver
341 substrates to proteases. For example, degradation of CtrA in *Caulobacter* is restricted to
342 the ClpXP protease via a highly regulated series of adaptors (Joshi et al., 2015).

343

344 In this work, we identified a mutant allele of *clpX* (*clpX**) that compensates for the loss
345 of Lon through expanding ClpXP substrate specificity (Figure 6D). The variant ClpX*P
346 protease complements the growth, motility, replication status, and morphology defects
347 of a Δ*lon* strain (Figure 1A-1C) by restoring levels and degradation of the Lon substrates
348 DnaA and SciP (Figure 2), which we confirm with biochemical experiments (Figure 3).
349 Interestingly, ClpX*P has an improved ability to degrade unfolded protein substrates, a
350 feature that likely explains the increased proteotoxic tolerance of Δ*lon clpX** strains
351 (Figure 3). Finally, this *clpX* variant is deficient in proteolysis of normal ClpXP
352 substrates, such as CtrA and ssrA-tagged proteins, suggesting a shift in substrate
353 preference rather than just an expansion (Figure 4, 6D). Mechanistic enzymology
354 revealed that ClpX* requires ~5-fold more ATP for saturation of ATP hydrolysis (Figure
355 5A), leading us to explore the role of ATP levels in controlling specificity. Surprisingly,
356 our *in vitro* studies found that wildtype ClpXP is better at degrading unfolded proteins,
357 DnaA, and SciP in ATP limiting conditions, but worse at degrading ssrA-tagged
358 proteins, similar to the behavior of ClpX*P even in saturating ATP conditions (Figure 5B,
359 5D, 6D, S5D). *In vivo*, DnaA degradation by wildtype ClpXP is accelerated (Figure 5E)
360 in starvation conditions that also deplete ATP. We speculate that the features which
361 alter ClpX* specificity even in high ATP conditions may also underlie the same change
362 in specificity seen with wildtype ClpX under low ATP conditions.
363

364 How does altered ATP levels or altered ability to use ATP change ClpX substrate
365 recognition? One model builds on emerging cryo-EM structures which have revealed
366 shared features of substrate-bound AAA+ complexes, namely a shallow right-handed
367 ring with pore loops gripping the substrate and at least 4 ATP-bound protomers (Fei et
368 al., 2020; Gates et al., 2017; Lopez et al., 2020; Ripstein et al., 2020; Shin et al., 2020).
369 Substrate-free forms of these machines show more open, often left-handed, spiral
370 structures (Shin et al., 2020; Yokom et al., 2016). Our limited proteolysis experiments,
371 which show faster chymotrypsin cleavage kinetics for ClpX* and wildtype ClpX at low
372 ATP, suggest that they adopt distinct conformations from wildtype ClpX at saturating

373 ATP (Figure 6A). Using HDX-MS, we find regions of ClpX* that show faster exchange
374 than wildtype ClpX at saturating ATP (Figure 6C, Figure S6A).
375
376 One possible model that arrives from these results is that ClpX normally samples
377 an 'open' state and a 'closed' state dependent on ATP levels. The 'closed' state is the
378 right-handed structure found in previous ClpXP structures (Fei et al., 2020; Ripstein et
379 al., 2020), while the 'open' state would be more similar to the left-handed spiral
380 structures found in substrate-free complexes (Shin et al., 2020; Yokom et al., 2016).
381 We modeled this open state for ClpX by aligning six ClpX monomers with the AAA
382 domains of substrate-free Lon from *Yersinia pestis* (Protein Data Bank ID: 6V11; Shin et
383 al., 2020). The peptide corresponding to residues 186-200 was no longer buried in this
384 modeled structure, consistent with a model where ClpX* can more readily adopt an
385 open state (Figure S6D). In this case, limiting ATP or appropriate mutations can shift the
386 open/closed balance toward the open state, which allows ClpX to better capture certain
387 substrates, such as unfolded proteins, that may not have as strict sequence
388 requirements for recognition (Figure S6E). However, degrons such as the ssrA tag
389 which bind selectively to the closed conformation (Hersch et al., 2005) would be poorly
390 recognized in these conditions (Figure S6E).
391
392 Alternatively, the changes in substrate specificity for ClpX* in saturating ATP
393 conditions and wildtype ClpX under low ATP conditions could be due to entirely distinct
394 mechanisms. For example, under low ATP concentrations, the ClpX oligomer is likely
395 unstable. As evidence of this, our DSF experiments show additional destabilization of
396 ClpX in low ATP conditions compared to either ClpX* and ClpX at saturating ATP
397 (Figure 6B). Similarly, using HDX-MS, we observed that ClpX in low ATP conditions
398 shows faster exchange across the entire sequence of ClpX in comparison to ClpX at
399 high ATP (Figure S6A). The destabilization of the ClpX hexamer could be underlying the
400 decreased GFP-ssrA degradation observed upon limiting ATP. However, this model
401 does not explain why ClpX under limited ATP conditions degrades FITC-Casein, DnaA,
402 and SciP better than at saturating ATP. Another possibility could be that ATP directly
403 competes with these substrates for degradation. In this case, intermediate nucleotide

404 concentrations provide enough ATP to power degradation and to also relieve inhibition,
405 allowing ClpX to degrade these substrates. However, to date, there is no evidence that
406 nucleotides directly compete with protein substrates for ClpX.
407
408 Prior work has shown that limiting nucleotide leads to loss of substrate
409 degradation by ClpXP (Martin et al., 2008), as would make sense for an ATP-fueled
410 unfoldase. We note that these studies exclusively used ssrA-tagged substrates, which
411 require an ATP-bound ('closed') form of ClpX for recognition (Martin et al., 2008). Thus,
412 the equivalent effects we are seeing here for casein, DnaA, and SciP would not have
413 been previously observed, which highlights the importance of using a range of
414 substrates in understanding activity. In our current work, we speculate that different
415 states of ClpX, favored by either limiting ATP or mutation, can result in meaningful
416 biological consequences. Intriguingly, similar conclusions were drawn for the
417 chaperonin GroEL, where mutants with a shifted specificity that improves folding of one
418 class of clients at the expense of others also resulted in an altered ATPase cycle
419 attributed to changes in conformational lifetimes (Wang et al., 2002). Overall, it seems
420 that exclusive substrate profiles for AAA+ systems are not hard-wired but can be altered
421 not only by mutations but also through modulation of ATP hydrolysis, demonstrating a
422 plasticity in these machines that yield flexibility in maintaining cellular proteostasis.
423
424 **Limitations of the study**
425 While our final model that ATP affects the dynamics of open/closed states of ClpX
426 oligomers satisfies our biochemical and cellular results, we acknowledge that there are
427 limitations in the experimental support of our model. One of the major concerns is that
428 ClpX oligomerization is ATP dependent, therefore under reduced ATP conditions the
429 partial dissociation of ClpX into inactive monomers is a confounding factor in our
430 interpretation of the results. A second concern is that although we favor a model where
431 ClpX* at saturating ATP mimics wildtype ClpX under limiting ATP in terms of the
432 mechanisms leading to shifted substrate specificity, it is possible that ClpX* has shifted
433 substrate preference for a reason completely different than why wildtype ClpX under
434 limiting ATP conditions has a similar shifted specificity. Because we have not directly

435 measured ATP stoichiometry, we also cannot say for certain whether ClpX or ClpX*
436 differ in nucleotide occupancy at saturating ATP concentrations. Finally, although open
437 apo-state spirals and closed substrate-bound rings have been found for several AAA+
438 family members (as described above), these have yet to be directly seen for ClpX.
439

440 **Acknowledgements**
441 We thank the Chien, Strieter, Stratton, and Serio lab members for helpful comments
442 and discussion on the manuscript. S.A.M. and B.A. were supported in part through
443 the UMass NIH Chemistry Biology Interface Training Program (NIH T32GM008515),
444 S.A.M. in part by the HHMI Gilliam Fellowship program, and B.A. in part by NIH
445 R01GM135931. Work in the Chien lab is funded by the NIH (R35GM130320). We thank
446 the Genomics Resource Laboratory (Institute for Applied Life Sciences; University of
447 Massachusetts Amherst) and the University of Massachusetts Mass Spectrometry Core
448 Facilities (RRID:SCR_019063) for services and equipment support.

449 **Author Contributions**: Conceptualization: S.A.M. and P.C.; Investigation, S.A.M. and
450 B.A.; Writing, S.A.M and P.C.; Funding Acquisition, P.C. Supervision, P.C.

451 **Declaration of Interests:** The authors declare no competing interests
452
453
454
455
456 **Main Text Figure Legends**
457

458 **Figure 1: *clpX** mutant suppresses *Δlon* phenotypes**
459 A. Growth curves of *wild type* (*wt*), *Δlon, and Δlon clpX** cells grown in PYE. Biological
460 triplicate experiments are shown. Error bars represent 95% confidence interval. Inset
461 shows motility assays as measured by growth in 0.3% PYE agar.
462 B. Representative phase-contrast microscopy images of *wt*, *Δlon, and Δlon clpX** cells
463 grown in PYE during exponential phase. Quantification of cell length and stalk length for
464 three biological replicates of n=100 cells.
465 C. Serial dilution assays comparing colony formation of strains in PYE and PYE
466 supplemented with mitomycin C. Spots are plated 10-fold dilutions of exponentially
467 growing cells from left to right.
468 D. Flow cytometry profiles showing chromosome content of indicated strains after three-
469 hour treatment with rifampicin. Cells were stained with SYTOX Green to measure DNA
470 content. The fluorescent intensities corresponding to one chromosome (1) and two

471 chromosomes (2) are indicated. Experiment was performed two times. Representative
472 data from one of the biological replicates is shown here.
473 E. Venn diagram summarizing the number of differentially expressed genes with an
474 FDR cutoff < 0.01 from RNA seq performed with stationary phase cells. Venn diagram
475 created by BioVenn (Hulsen, de Vlieg and Alkema, 2008).
476
477 See also Figure S1 and Supplementary File 1.
478
479
480 **Figure 2: *clpX** mutant restores levels of Lon substrates through degradation**
481 A. Lon degrades DnaA, SciP, and CcrM in *C. crescentus* (Wright *et al.*, 1996; Gora *et*
482 *al.*, 2013; Jonas *et al.*, 2013).
483 B. Western blot showing DnaA and CcrM levels in *wt*, *Δlon, and Δlon clpX** cells.
484 Lysates from an equal number of exponential phase cells were probed with anti-DnaA
485 or anti-CcrM antibody. ClpP was used as a loading control. A representative image and
486 quantifications of triplicate experiments are shown. Line represents the mean.
487 C. Antibiotic shutoff assays to monitor DnaA and CcrM stabilities in wt*, Δlon, and Δlon*
488 *clpX** cells. Chloramphenicol was added to stop synthesis and lysates from samples at
489 the indicated time points were used for western blot analysis. Quantifications of triplicate
490 experiments with substrate shown relative to ClpP control levels are shown to the right.
491 Error bars represent SD.
492 D. Western blot showing SciP levels in synchronized populations of wt, *Δlon, and Δlon*
493 *clpX** cells. Swarmer cells were isolated using a density gradient and an equal number
494 of cells were released into fresh PYE medium. Samples were withdrawn at the indicated
495 time points and probed with anti-SciP.
496 E. DnaA stability is measured in Δ*lon* strains expressing an extra copy of wildtype *clpX*
497 or *clpX**. Experiment was performed four times. Representative data from one of the
498 biological replicates is shown here. Quantifications of experiments shown to the right.
499 Error bars represent SD.
500
501 See also Figure S2.
502
503
504 **Figure 3: ClpX*P degrades some Lon substrates faster than ClpXP *in vitro*.**
505 A. *In vitro* degradation of DnaA, SciP, or CcrM. Assays were performed with 0.1 μM
506 $ClpX_6$ or $ClpX_6$*, and 0.2 μM $ClpP_{14}$. Substrate concentrations were 1 μM DnaA, 5 μM
507 SciP, 0.5 μM CcrM. Quantification of triplicate experiments shown. Error bars represent
508 SD.
509 B. *In vitro* fluorescence degradation assay of FITC-casein in the presence of ClpXP or
510 ClpX*P or Lon. Degradation assays were performed with 10μg/mL FITC-Casein, 0.1 μM
511 $ClpX_6$ or $ClpX_6$* and 0.2 μM $ClpP_{14}$ or 0.1 μM Lon_6. Serial dilution assays comparing
512 colony formation of strains in PYE and PYE supplemented with L-canavanine. Spots are
513 plated 10-fold dilutions of exponentially growing cells from left to right.
514
515 See also Figure S3.
516

517
518 **Figure 4: ClpX* mutant is deficient in degradation of native ClpXP substrates**
519 A. Michaelis-Menten plot showing the rate of degradation as a function of GFP-ssrA
520 concentration by ClpXP and ClpX*P. Inset displays kinetic parameters. Assays were
521 performed with 0.1 μM $ClpX_6$ or $ClpX^*_6$, 0.2 μM $ClpP_{14}$, ATP regeneration system, and
522 the indicated concentrations of GFP-ssrA. Data was fitted to Michaelis-Menten
523 equation. Triplicate experiments are shown.
524 B. *In vitro* degradation assay of His-CtrA in the presence of ClpXP or ClpX*P.
525 Degradation assays were performed with 3 μM His-CtrA, 0.1 μM $ClpX_6$ or $ClpX^*_6$, 0.2
526 μM $ClpP_{14}$, and ATP regeneration system. Quantification of duplicate experiments is
527 shown below. Error bars represent SD.
528 C. *In vivo* degradation assay showing eGFP-ssrA (DAS), DnaA, and CtrA stability in *wt*
529 and *clpX** cells. The plasmid encoded M2FLAG-eGFP-ssrA (DAS) construct was
530 induced with the addition of 0.2% xylose. Chloramphenicol was used to inhibit protein
531 synthesis. Samples were withdrawn at the indicated time points and quenched in SDS
532 lysis buffer. Lysate from an equal number of cells was used for western blot analysis
533 and probed with anti-M2, or anti-CtrA, and anti-DnaA antibody. Quantification of
534 triplicate experiments is shown below. Error bars represent SD.
535 D. Competition assay with wildtype cells harboring xylX::Plac-venus (constitutive venus
536 expression) and nonfluorescent wt or *clpX** strains. exponential phase cells were mixed
537 1:1, diluted, and allowed to outgrow for 12 doublings. Quantification of triplicate
538 experiments is shown below. Error bars represent SD.
539 E. Serial dilution assays comparing colony formation of *wt* and *clpX** cells in PYE and
540 PYE supplemented with MMC. Spots are plated 10-fold dilutions of exponentially
541 growing cells from left to right.
542
543 See also Figure S4.
544
545

546 **Figure 5: Limiting ATP alters wildtype ClpXP substrate specificity**

547 A. Michaelis-Menten plot showing the rate of ClpX/ClpX* catalyzed ATP hydrolysis as a
548 function of ATP concentration. Inset displays kinetic parameters. Assays were
549 performed with 0.1 μM $ClpX_6$ or $ClpX^*_6$, in the presence and absence of 0.2 μM $ClpP_{14}$.
550 Data was fitted to Michaelis-Menten equation. Triplicate experiments are shown.
551 B. FITC-Casein degradation by ClpXP or ClpX*P as a function of ATP concentration.
552 Assays were performed with 0.1 μM $ClpX_6$ or $ClpX^*_6$, 0.2 μM $ClpP_{14}$, ATP regeneration
553 system, and 50 μg/mL FITC-Casein. Rates were normalized to highest concentration of
554 ATP. Non-normalized rates shown in the inset.
555 C. Michaelis-Menten plot showing the rate of degradation as a function of FITC-Casein
556 concentration by ClpXP under low and saturating ATP conditions. Inset displays kinetic
557 parameters. Assays were performed with 0.1 μM $ClpX_6$, 0.2 μM $ClpP_{14}$, and ATP
558 regeneration system. Data was fitted to Michaelis-Menten equation. Triplicate
559 experiments are shown.

560 D. *In vitro* degradation of DnaA by ClpXP under low and saturating ATP conditions.
561 Assays were performed with 0.1 μM $ClpX_6$, and 0.2 μM $ClpP_{14}$ and 0.5 μM DnaA.
562 Quantification of triplicate experiments.
563 E. Antibiotic shutoff assays to monitor DnaA under ATP limiting conditions in *wt* and
564 *Δlon ΔclpA* strains. Chloramphenicol was added to stop synthesis and lysates from
565 samples at the indicated time points were used for western blot analysis. Quantifications
566 of triplicate experiments shown to the right. Error bars represent SD.
567
568 See also Figure S5.
569
570 **Figure 6: ClpX adopts distinct ATP-dependent conformational states**
571 A. Limited proteolysis assay to probe conformational states. ClpX was incubated with
572 Chymotrypsin with either 12 μM ATP or 4 mM ATP in the presence of ClpP and ATP
573 regeneration system at 25 °C for the indicated time points. ClpX* was incubated with
574 Chymotrypsin at 4 mM ATP in the presence of ClpP and ATP regeneration system at 25
575 °C for the indicated time points. ClpX was detected using anti-ClpX antibodies.
576 B. Stability of ClpX* with 4 mM ATP, ClpX with 4 mM ATP, and ClpX with 12 μM ATP as
577 measured by differential scanning fluorimetry. Triplicate experiments shown.
578 C. Woods plot comparing deuterium uptake for wildtype ClpX vs ClpX* at 4 mM ATP
579 after 60 minutes. Each bar on Woods plot represents a single peptide with peptide
580 length corresponding to the bar length. Red bars indicate a deprotected (more
581 deuterium uptake) region, blue represents a protected region, and gray bars are not
582 significantly different. Woods plots were created with Deuteros (Lau et al. 2021) using
583 the peptide significance test (p-value <0.01). Residues 186-200 are highlighted in red
584 for the equivalent residues in the substrate-bound *E. coli* ClpX structure (Protein Data
585 Bank ID: 6PO1) using PYMOL (Schrodinger).
586 D. In a wildtype cell, AAA+ proteases Lon and ClpXP promote normal growth by
587 degrading distinct substrates. ClpX*P can compensate for the absence of the Lon
588 protease by tuning ClpX substrate specificity to better degrade Lon-restricted substrates
589 (such as DnaA, SciP, and misfolded proteins) but this comes at the cost of native ClpXP
590 substrates (such as ssrA-tagged proteins and CtrA). In ATP-limited conditions, wildtype
591 ClpXP can undergo a similar switch in substrate specificity to ClpX*P, gaining the ability
592 to better degrade DnaA, SciP, and misfolded proteins than the wildtype enzyme at
593 saturating ATP.
594
595 See also Figure S6.
596
597
598
599
600
601
602
603

604 **STAR Methods**

605 **RESOURCE AVAILABILITY**

606

607 **Lead Contact**

608 - Further information and requests for resources and reagents should be directed
609 to and will be fulfilled by the Lead Contact, Peter Chien (pchien@umass.edu).

610

611 **Materials Availability**

612 - All unique/stable reagents generated in this study are available from the Lead
613 Contact without restriction.

614 **Data and Code Availability**

615 - RNAseq data are available in the NCBI Gene Expression Omnibus
616 (GEO): GSE166765
617 (https://www.ncbi.nlm.nih.gov/geo/query/acc.cgi?acc=GSE166765)
618 - This paper does not report original code.
619 - Any additional information required to reanalyze the data reported in this paper is
620 available from the lead contact upon request.

621 **EXPERIMENTAL MODEL AND SUBJECT DETAILS**

622

623 **Bacterial strains**

624 Bacterial strains used in this study are listed in the key resources table. *Caulobacter*
625 *crescentus* strains were grown in PYE medium (2g/L peptone, 1g/L yeast extract, 1 mM
626 $MgSO_4$, and 0.5 mM $CaCl_2$) at 30°C and supplemented with antibiotics at the following
627 concentrations: kanamycin (25 µg/ml), spectinomycin (100 µg/ml), and oxytetracycline
628 (2 µg/ml). After initial selection steps for strain construction (excluding plasmids),
629 antibiotics were excluded for all assays.

630

631 *Escherichia coli* strains were grown in LB (10g/L NaCl, 10g/L tryptone, 5g/L yeast
632 extract) and supplemented with antibiotics at the following concentrations: ampicillin
633 (100 ug/ml), oxytetracycline (15 µg/ml), spectinomycin (50 µg/ml), kanamycin (50

634 μg/ml), gentamycin (20 μg/ml). For solid medium, 1.5% agar was used regardless of
635 bacterial species. For all strains, optical density was measured at 600 nm.
636
637 For induction purposes, the 477 plasmids were induced with xylose (0.2%) and
638 repressed with glucose (0.2%). For protein expression, 0.4 mM IPTG was used for
639 induction.
640
641 **METHOD DETAILS**
642
643 **Cloning and strain constructions**
644 All *Caulobacter* strains were derived from CPC176, an isolate of NA1000. To generate
645 the *Δlon clpX** strain, a two-step recombination protocol with a sucrose counter
646 selection was utilized (Skerker et al., 2005). The vector pNPTS138 was digested with
647 HindIII and EcoRI. A PCR product of the *clpX** sequence was amplified from the original
648 motility suppressor and Gibson assembly was then used to generate pNPTS138_clpX*.
649 Following transformation with pNPTS138_clpX* into NA1000 or *Δlon*, primary selection
650 was on PYE supplemented with kanamycin. Primary colonies were grown overnight
651 without selection and overnight cultures were played on PYE agar supplemented with
652 3% w/v sucrose. To validate allelic swap, strains were tested for sensitivity to
653 kanamycin. *Δlon clpX** was also screened by motility and sequencing of the *clpX* locus
654 validated candidate clones.
655
656 *ClpX* or *clpX** merodiploid strains were generated by Gibson assembly of PCR product
657 and double digested plasmids of pMCS-2. The plasmids were then electroporated into
658 *Δlon* and selected onto kanamycin plates. Strains were validated by anti-ClpX westerns.
659
660 eGFP-ssrA(DAS) induction strains were generated by electroporating eGFP-ssrA(DAS)
661 477 plasmid into wildtype and wildtype *clpX** and selecting on spectinomycin. Strains
662 were validated by anti-M2 westerns.
663
664 **Motility suppressor screen**

665 Transposon libraries were generated for *Δlon*. Two-liter PYE cultures were grown to mid
666 exponential phase, pelleted, and washed with 10% glycerol. Competent cells were
667 electroporated with Ez-Tn5 <Kan-2> transposome (Lucigen, Madison, WI). Cells
668 recovered for 90 minutes at 30 °C and then played on PYE plates supplemented with
669 kanamycin. Libraries were grown for 7 days. Colonies were then scraped from the
670 surface, combined, and resuspended to form a homogenous solution of PYE + 20%
671 glycerol.
672
673 The Tn library was thawed out and diluted into a flask containing two-liter 0.3% agar.
674 The cell agar mixture was plated and grown at 30 °C for 3 to 5 days. Candidates that
675 appeared motile were validated by inoculating single colonies into motility agar on the
676 same plate as NA1000 as a positive control and Δ*lon* as a negative control and
677 incubating plates for 2-3 days at 30 °C.
678
679 **Motility assay**
680 A single colony was inoculated into PYE with 0.3% agar using a sterile pipette tip and
681 left to incubate at 30°C for 2 to 3 days.
682
683 **Whole genome sequencing**
684 Genomic DNA was extracted using the MasterPure Complete DNA and RNA
685 purification kit (Epicenter Biotechnologies, Madison, WI). A Qubit Fluorometer
686 (ThermoFisher Scientific, Waltham, MA) was utilized to assess DNA concentration.
687 Illumina libraries were generated from the extracted genomic DNA using the NexteraXT
688 (Illumina, San Diego, CA) protocol. Libraries were multiplexed and sequenced at the
689 University of Massachusetts Amherst Genomics Core Facility on the NextSeq 500
690 (Illumina). Single nucleotide polymorphisms (SNPs) were detected using breseq
691 (Deatherage and Barrick, 2014).
692
693 **RNA sequencing**
694 RNA was extracted from stationary phase cells. Libraries were generated from the
695 extracted RNA using the NEB Next RNA Library Prep kits (NEB, Ipswich, MA). Libraries

696 were sequenced at the University of Massachusetts Genomics Core Facility on the
697 NextSeq 500 with single end 75 base reads.
698
699 **Plating viability and drug sensitivity**
700 All *Caulobacter* strains were grown overnight in liquid PYE media. After overnight
701 growth, cells were back diluted to OD600 0.1 and outgrown to mid-exponential phase
702 before being normalized to OD_{600} 0.1 and 10-fold serially diluted on to media. For
703 experiments using mitomycin C (Sigma, St. Louis, MO) and L-canavanine (Sigma),
704 drugs were prepared at a stock concentration of 400 µg/ml mitomycin C, and 100 mg/ml
705 L-canavanine and filter sterilized. PYE agar was cooled before the drugs were added
706 and plates were left to air dry prior to serial dilution plating. All plates were incubated at
707 30℃ for 2-3 days and imaged with a Syngene G:Box.
708
709 ***In vivo* assays**
710 The stability of proteins *in vivo* was determined by inhibiting protein synthesis upon
711 addition of 30 µg/ml chloramphenicol to cells in exponential phase. At each time point,
712 1ml of culture was removed and centrifuged at 15,000 rpm for 2 minutes. The
713 supernatant was removed and pellets were flash frozen in liquid nitrogen. Pellets were
714 thawed, resuspended in 2x SDS dye, and normalized to the OD_{600} of the lowest sample.
715 Samples were boiled for 10 minutes and centrifuged for 10 minutes at 15,000 rpm.
716 Extracts were run on 10% Bis-Tris gels for 1 hour at room temperature at 150 V. Gels
717 were then transferred to nitrocellulose membranes for 1 hour at room temperature at
718 20V. Membranes were blocked with 3% milk in Tris-based saline with 0.05% Tween-20
719 (TBST) for 1 hour. Membranes were probed with primary antibody in 3% milk in TBST
720 at 4°C overnight with following dilution factors: 1:5000 dilution of DnaA, 1:5000 SciP,
721 1:5000 CcrM, 1:5000 ClpP, 1:2500 Lon, and 1:2000 M2. Membranes were washed with
722 1x TBST for 5 minutes three times and then probed with Licor secondary antibody with
723 1:10,000 dilution in 1x TBST at room temperature for 1 hour.
724

725 To synchronize *Caulobacter* strains, cells were grown to an OD600 of 0.3-0.5 in PYE
726 and swarmer cells were isolated using Percoll density centrifugation. Cells were
727 released into PYE.

728 Flow cytometry was used to measure DNA content in rifampicin-treated cells as
729 previously described (Chen et al., 2009). Cells were treated with rifampicin for three
730 hours prior to fixing in 70% ethanol.

731 **Carbon starvation**

732 Cells were grown in M2G media (6.1 mM Na_2HPO_4, 3.9 mM KH_2PO_4, 9.3 mM NH_4Cl,
733 0.5 mM $MgSO_4$, 0.5 mM CaCl2, 10 μM $FeSO_4$ (EDTA chelate), 0.2% glucose). Cells
734 were then washed twice in cold M2G media (+glucose samples) or in M2 media (-
735 glucose samples) and resuspended in pre-warmed M2G or M2 media.

736 **Growth competition assay**

737 Overnight cultures of CPC798 were mixed with either *NA1000* or *clpX** at a 1:1 ratio.
738 For competition assays with *Δlon* strains, overnight cultures of CPC807 were mixed with
739 either *Δlon* or *Δlon clpX** at a 1:1 ratio. Mixed strains were diluted into fresh PYE and
740 allowed to outgrow for 12 doublings overnight. The initial populations were verified by
741 phase contrast and fluorescent microscopy. Final ratios were normalized to their starting
742 ratios. Data was plotted using GraphPad Prism.

743 **Microscopy**

744 Phase contrast images of logarithmically growing cells were taken by Zeiss AXIO Scope
745 A1. Cells were mounted on 1% PYE agar pads and imaged using a 100X objective.
746 Representative images of the same scale were cropped to display morphological
747 defects.

748 **Protein purification and modification**

749 Untagged Lon, untagged ClpX and ClpX*, and his-tagged ClpP were purified as
750 previously described (Chien et al., 2007b; Goldberg et al., 1994; Gur and Sauer, 2008b;
751 Levchenko et al., 2000). Titin-I27-β20 was purified as previously described (Gur and
752 Sauer, 2008b; Kenniston et al., 2003) and labeled with Fluorescein-5-maleimide
753 (Thermo Scientific) under guanidine hydrochloride denaturation. The modified protein

754 was buffer exchanged into H-buffer (20 mM Hepes pH 7.5, 100 mM KCl, 10 mM MgCl2,
755 10% glycerol) and stored at 4°C. The concentration of fluorescein-modified Titin-I27-β20
756 was determined using the Bradford assay (Thermo Scientific). FITC-Casein (Type III,
757 Sigma) was prepared in water and stored at -20°C. His_6SciP and his_6CtrA were purified
758 as described in (Gora et al., 2013b). DnaA and CcrM were purified as his_6SUMO tagged
759 proteins, followed by tag cleavage as described (Jonas et al., 2013; Liu et al., 2016;
760 Wang et al., 2007). GFP-ssrA was purified as previously described (Yakhnin et al.,
761 1998). CtrA-RD+15 was purified as described (Smith et al., 2014b). Detailed purification
762 protocols are available upon request.
763
764 ***In vitro* reconstitution assays**
765 Degradation assays were performed at 30°C and monitored using SDS-PAGE gels as
766 described previously (Bhat et al., 2013). The final concentrations used can be found in
767 the figure legends.
768
769 **Limited proteolysis**
770 To perform limited chymotrypsin digestion, 0.004 mg/mL chymotrypsin was added to
771 0.01 mg/mL ClpX or ClpX* in the presence of ClpP and ATP regeneration system and
772 incubated at 25°C in Hepes buffer (20 mM Hepes pH 7.5, 100 mM KCl, 10 mM MgCl2,
773 10% glycerol) for indicated time points. To quench the reactions, 5X SDS dye
774 supplemented with 5 mM Protease inhibitor phenylmethylsulfonyl fluoride (PMSF) was
775 added. The samples were run on a 10% Bis-Tris gel and transferred to nitrocellulose as
776 described above. Membranes were probed with primary antibody in 3% milk in TBST at
777 4°C overnight with following dilution factors: 1:5000 dilution of ClpX. Membranes were
778 washed with 1x TBST for 5 minutes three times and then probed with Licor secondary
779 antibody with 1:10,000 dilution in 1x TBST at room temperature for 1 hour. The protein
780 was visualized using Licor Odyssey CLx.
781
782 **Binding of ADP to ClpX**
783

784 625 nM mant-ADP was pre-incubated with 300 nM $ClpX_6$/$ClpX_6$* for 10 minutes.
785 Subsequently, ATPγS was added to compete off the mant-ADP at various
786 concentrations. Polarization measurements were read from 20 uL of these mixtures
787 after an additional 15-minute incubation using opaque black NBS 384-well plates
788 (Corning) and a SpectraMax M5 plate reader (Molecular Devices), with excitation and
789 emission wavelengths set at 357 and 445 nm, respectively.
790
791 **Differential scanning fluorimetry**
792 Differential scanning fluorimetry was carried out in a Biorad realtime PCR thermocycler.
793 6 μM monomer of ClpX or ClpX* in the presence of 4 mM ATP or 12 μM ATP was mixed
794 in a 1:1 ratio with 4X Sypro Orange in Hepes Buffer (20 mM Hepes pH 7.5, 100 mM
795 KCl, 10 mM $MgCl_2$). The resulting mixtures were incubated at room temperature for 30
796 mins to allow the Sypro Orange to coat the proteins before subjecting triplicate samples
797 to thermal unfolding from 25 °C to 95 °C. Melting temperatures were calculated by fitting
798 of a 5-parameter sigmoid curve using the JTSA software (P. Bond,
799 https://paulsbond.co.uk/jtsa).
800
801 **Hydrogen-deuterium exchange mass spectrometry (HDX-MS)**
802 Hydrogen-deuterium exchange experiments were carried out on a Synapt G2Si high-
803 definition mass spectrometer (Waters) using an automated HDX robotics platform
804 (Waters). Samples of 5.4 μM ClpX or ClpX* monomer were diluted 1:16 in D_2O buffer
805 containing 20 mM Hepes, 10 mM $MgCl_2$, 100 mM KCl, and 5% glycerol. D_2O and H_2O
806 buffers were supplemented with 4 mM ATP plus regeneration system (30 mM creatine
807 kinase and 0.5 mg/mL creatine phosphate) for the high ATP condition and 12 μM ATP
808 for the low ATP condition. Deuterium exchange was allowed to take place for 0, 10
809 seconds, 1 min, 10 minutes, and 60 min at 25 °C. The samples were subsequently
810 quenched by addition of cold quench buffer (233 mM Sodium Phosphate pH 2.5) and
811 run over an immobilized Waters ENZYMATE immobilized pepsin column (inner
812 diameter: 2.1 × 30 mm) at a flow rate of 0.15 mL/min at high pressure (~11,000 psi) for
813 peptide digestion. Blank runs were run in between each analysis to avoid peptide carry
814 over. Continuous lock-mass correction was performed using leu-enkephalin compound.

815 Peptides were ionized and separated by electrospray ionization for analysis at a mass
816 resolution of 50 to 2,000 *m*/*z* range. Peptides were identified with triplicate undeuterated
817 samples from each condition. Specific peptide regions were mapped onto the
818 corresponding residues in the *E. coli* cryo-EM structure (PDB ID: 6PO1) using PYMOL
819 (Version 2.5.0, Schrödinger). A model of ClpX in the potential open state was created
820 by aligning each ClpX monomer to each ATPase monomer of the *Y. pestis* substrate-
821 free cryo-EM structure (PDB ID: 6V11) by using the align function in PYMOL.
822
823 **QUANTIFICATION AND STATISTICAL ANALYSIS**
824
825 Graphs were generated in GraphPad Prism. Unless otherwise stated in the figure
826 legend, results represent the mean ± Standard Deviation (SD). Sample sizes are also
827 reported in the figure notes. Error bars for the growth curves shown in Figure 1A
828 represent the 95% confidence interval.
829
830 **RNA sequencing data**
831
832 Reads were mapped to the *Caulobacter* genome using BWA (Li and Durbin, 2009) and
833 sorted with Samtools (Li et al., 2009).To obtain the number of reads per gene, *bedtools*
834 *map* (Quinlan and Hall, 2010) was used. Rstudio and EdgeR was used to identify
835 differentially expressed genes (R Core Team, 2019; Robinson et al., 2009).
836
837 Raw counts were normalized using the counts-per-million (CPM) method, and the
838 *edgeR* package in R was used to perform differential gene expression analysis, KEGG
839 pathway analysis, and FRY (Wu et al., 2010) gene set analysis. We filtered out any
840 gene that had less than 30 normalized counts across 3 or more samples. To test for
841 gene expression differences and identify differentially expressed genes across
842 experimental groups, we used the quasi-likelihood F-test. The over-representation
843 analysis for KEGG pathways done using the *kegga* function. FRY gene set analysis
844 done using the *fry* function. The CcrM, DnaA, and SciP regulons were obtained from
845 (Gonzalez et al., 2014; Hottes et al., 2005; Tan et al., 2010).

846

847 ***In vivo* assays**

848

849 For western blots, proteins were visualized using Licor Odyssey CLx. Bands were
850 quantified using ImageJ (NIH) and degradation rates were plotted using Prism
851 (Graphpad).

852

853 For bulk measurements of intracellular ATP, the Bactiter-Glo microbial cell viability
854 assay kit (Promega) was used. Cells were mixed with an equal volume of BacTiter-Glo
855 reagent in 384-well microtiter plates and incubated for five minutes before luminescence
856 was measured.

857

858 For microscopy, MicrobeJ (Ducret et al., 2016) for ImageJ (Schneider et al., 2012) was
859 utilized to quantify cell lengths. Stalk lengths were quantified using ImageJ. Prism was
860 utilized for representations of cell and stalk length measurements.

861

862 ***In vitro* assays**

863 Densitometry for degradation assays was performed with ImageJ and degradation rates
864 were plotted using Prism.

865

866 Degradation of FITC-Casein and FT-Titin-B20 was monitored as an increase in
867 fluorescence over time. GFP-CtrARD+15 degradation was observed as a loss of
868 fluorescence over time as described previously (Smith et al., 2014b).

869

870 ATP hydrolysis for ClpXP and ClpX*P was measured using a coupled kinase assay as
871 previously described (Burton et al., 2003).

872

873 For binding of ADP to ClpX, IC50s were calculated by fitting the polarization data using
874 GraphPad Prism to an inhibitor versus response – variable slope (four paramaters)
875 function in GraphPad Prism: Y=Bottom + (Top-Bottom)/(1+(IC50/X)^HillSlope) where
876 IC50 is the ATPγS concentration halfway between bottom and top.

For differential scanning fluorimetry, melting temperatures were calculated by fitting of a 5-parameter sigmoid curve using the JTSA software (P. Bond, https://paulsbond.co.uk/jtsa).

HDX-MS data

HDX-MS experiments were performed in triplicate. Identification of peptides and analysis of the uptake plots and charge states for each peptide were completed in Protein Lynx Global Server and DynamX (v. 3.0, Waters). The following processing paramaters were utilized: minimum peptide intensity of 1000, minimum peptide length of 5, maximum peptide length of 30, minimum MS/MS products of 2, minimum products per amino acid of 0.25, minimum score of 5, and maximum MH+ error threshold of 15 p.p.m. Woods plots were generated by Deuteros (Lau et al., 2021) using the peptide significance test (p-value <0.01). HDX data summary for each condition was exported from Deuteros and can be found in Supplementary File 3. No correction was made for back-exchange.

Descriptive titles for Supplemental Files

DataS1. This file contains the RNA sequencing experiments referred to in Main Figure 1. DataS1.xlsx

DataS2. This file contains the Hydrogen Deuterium Exchange log for experiments shown in Main Figure 6. DataS2.pdf

914
915 **References**
916
917 Baker, T.A., and Sauer, R.T. (2012). ClpXP, an ATP-powered unfolding and protein-
918 degradation machine. Biochim Biophys Acta Mol Cell Res *1823*, 15–28.
919
920 Bhat, N.H., Vass, R.H., Stoddard, P.R., Shin, D.K., and Chien, P. (2013). Identification
921 of ClpP substrates in Caulobacter crescentus reveals a role for regulated proteolysis in
922 bacterial development. Mol. Microbiol. *88*, 1083–1092.
923
924 Breidenstein, E.B.M., Janot, L., Strehmel, J., Fernandez, L., Taylor, P.K., Kukavica-
925 Ibrulj, I., Gellatly, S.L., Levesque, R.C., Overhage, J., and Hancock, R.E.W. (2012). The
926 Lon Protease Is Essential for Full Virulence in Pseudomonas aeruginosa. PLoS ONE *7*.
927
928 Chen, Y.E., Tsokos, C.G., Biondi, E.G., Perchuk, B.S., and Laub, M.T. (2009).
929 Dynamics of two phosphorelays controlling cell cycle progression in Caulobacter
930 crescentus. J. Bacteriol. *191*, 7417–7429.
931
932 Chien, P., Perchuk, B.S., Laub, M.T., Sauer, R.T., and Baker, T. (2007). Direct and
933 adaptor-mediated substrate recognition by an essential AAA+ protease. Proc. Natl.
934 Acad. Sci. U. S. A. *104*, 6590–6595.
935
936 Chowdhury, T., Chien, P., Ebrahim, S., Sauer, R.T., and Baker, T.A. (2010). Versatile
937 modes of peptide recognition by the ClpX N domain mediate alternative adaptor-binding
938 specificities in different bacterial species. Protein Sci. *19*, 242–254.
939
940 Deatherage, D.E., and Barrick, J.E. (2014). Identification of mutations in laboratory
941 evolved microbes from next-generation sequencing data using breseq. Methods Mol
942 Biol. 165–188.
943
944 Domian, I.J., Reisenauer, a, and Shapiro, L. (1999). Feedback control of a master
945 bacterial cell-cycle regulator. Proc. Natl. Acad. Sci. U. S. A. *96*, 6648–6653.
946
947 Doyle, S.M., Shorter, J., Zolkiewski, M., Hoskins, J.R., Lindquist, S., and Wickner, S.
948 (2007). Asymmetric deceleration of ClpB or Hsp104 ATPase activity unleashes protein-
949 remodeling activity. Nat. Struct. Mol. Biol *14*, 114–122.
950
951 Ducret, A., Quardokus, E.M., and Brun, Y. V. (2016). MicrobeJ, a tool for high
952 throughput bacterial cell detection and quantitative analysis. Nat. Microbiol. *1*, 1–7.
953
954 Evinger, M., and Agabian, N. (1977). Envelope-associated nucleoid from Caulobacter
955 crescentus stalked and swarmer cels. J. Bacteriol. *132*, 294-301.
956
957 Farrell, C.M., Baker, T.A., and Sauer, R.T. (2007). Altered Specificity of a AAA+
958 Protease. Mol. Cell *25*, 161–166.
959

960 Fei, X., Bell, T.A., Barkow, S.R., Baker, T.A., and Sauer, R.T. (2020). Structural basis of
961 clpxp recognition and unfolding of ssra-tagged substrates. ELife *9*, 1–39.
962
963 Gates, S.N., Yokom, A.L., Lin, J., Jackrel, M.E., Rizo, A.N., Kendsersky, N.M., Buell,
964 C.E., Sweeny, E.A., Mack, K.L., Chuang, E., et al. (2017). Ratchet-like polypeptide
965 translocation mechanism of the AAA+ disaggregase Hsp104. Science *357*, 273–279.
966
967 Goff, S.A., Casson, L.P., and Goldberg, A.L. (1984). Heat shock regulatory gene htpR
968 influences rates of protein degradation and expression of the lon gene in Escherichia
969 coli. Proc. Natl. Acad. Sci. U. S. A. *81*, 6647–6651.
970
971 Goldberg, A.L. (1972). Degradation of Abnormal Proteins in Escherichia coli. Proc Natl
972 Acad Sci U. S. A. *69*, 422–426.
973
974 Goldberg, A.L., Moerschell, R.P., Hachung, C., and Maurizi, M.R. (1994). ATP-
975 dependent protease La (Lon) from Escherichia coli. Meth. Enzymol. *244*, 350–375.
976
977 Gonzalez, D., Kozdon, J.B., McAdams, H.H., Shapiro, L., and Collier, J. (2014). The
978 functions of DNA methylation by CcrM in Caulobacter crescentus: A global approach.
979 Nucleic Acids Res. *42*, 3720–3735.
980
981 Gora, K.G., Cantin, A., Wohlever, M., Joshi, K.K., Perchuk, B.S., Chien, P., and Laub,
982 M.T. (2013). Regulated proteolysis of a transcription factor complex is critical to cell
983 cycle progression in Caulobacter crescentus. Mol. Microbiol. *87*, 1277–1289.
984
985 Gorbatyuk, B., and Marczynski, G.T. (2005). Regulated degradation of chromosome
986 replication proteins DnaA and CtrA in Caulobacter crescentus. Mol. Microbiol. *55*, 1233–
987 1245.
988
989 Gottesman, S., Roche, E., Zhou, Y.N., and Sauer, R.T. (1998). The ClpXP and ClpAP
990 proteases degrade proteins with carboxy-terminal peptide tails added by the SsrA-
991 tagging system. Genes Dev. *12*, 1338–1347.
992
993 Gur, E., and Sauer, R.T. (2008). Recognition of misfolded proteins by Lon, a AAA+
994 protease. Genes Dev. *22*, 2267–2277.
995
996 Gur, E., Biran, D., and Ron, E.Z. (2011). Regulated proteolysis in Gram-negative
997 bacteria — how and when? Nat Rev Microbiol *9*, 839–848.
998
999 Hersch, G.L., Burton, R.E., Bolon, D.N., Baker, T.A., and Sauer, R.T. (2005).
1000 Asymmetric interactions of ATP with the AAA+ ClpX6 unfoldase: Allosteric control of a
1001 protein machine. Cell *121*, 1017–1027.
1002
1003 Hottes, A.K., Shapiro, L., and McAdams, H.H. (2005). DnaA coordinates replication
1004 initiation and cell cycle transcription in Caulobacter crescentus. Mol. Microbiol. *58*,
1005 1340–1353.

1006
1007 Howard-Flanders, P., Simson, E., and Theriot, L. (1964). A locus that controls filament
1008 formation and sensitivity to radiation in Escherichia coli K-12. Genetics *49*, 237–246.
1009
1010 Jenal, U., and Fuchs, T. (1998). An essential protease involved in bacterial cell-cycle
1011 control. EMBO J. *17*, 5658–5669.
1012
1013 Jonas, K., Liu, J., Chien, P., and Laub, M.T. (2013). Proteotoxic stress induces a cell-
1014 cycle arrest by stimulating lon to degrade the replication initiator DnaA. Cell *154*, 623–
1015 636.
1016
1017 Joshi, K.K., Bergé, M., Radhakrishnan, S.K., Viollier, P.H., and Chien, P. (2015). An
1018 Adaptor Hierarchy Regulates Proteolysis during a Bacterial Cell Cycle. Cell *163*, 419–
1019 431.
1020
1021 Keiler, K.C. (2015). Mechanisms of ribosome rescue in bacteria. Nat. Rev. Microbiol.
1022 *13*, 285–297.
1023
1024 Keiler, K.C., Waller, P.R.H., and Sauer, R.T. (1996). Role of a Peptide Tagging System
1025 in Degradation of Proteins Synthesized from Damaged Messenger RNA. Science *271*,
1026 990–993.
1027
1028 Kenniston, J.A., Baker, T.A., Fernandez, J.M., and Sauer, R.T. (2003). Linkage between
1029 ATP consumption and mechanical unfolding during the protein processing reactions of
1030 an AAA+ degradation machine. Cell *114*, 511–520.
1031
1032 Kim, D.Y., and Kim, K.K. (2003). Crystal Structure of ClpX Molecular Chaperone from
1033 Helicobacter pylori. J. Biol. Chem. *278*, 50664–50670.
1034
1035 Langklotz, S., Baumann, U., and Narberhaus, F. (2012). Structure and function of the
1036 bacterial AAA protease FtsH. Biochim Biophys Acta Mol Cell Res *1823*, 40–48.
1037
1038 Lau, A.M., Claesen, J., Hansen, K., and Politis, A. (2021). Deuteros 2.0: Peptide-level
1039 significance testing of data from hydrogen deuterium exchange mass spectrometry.
1040 Bioinformatics *37*, 270–272.
1041
1042 Lau, J., Hernandez-Alicea, L., Vass, R.H., and Chien, P. (2015). A phosphosignaling
1043 adaptor primes the AAA+ protease ClpXP to drive cell cycle regulated proteolysis. Mol.
1044 Cell. *59*, 104-16.
1045
1046 Laub, M.T., Chen, S.L., Shapiro, L., and McAdams, H.H. (2002). Genes directly
1047 controlled by CtrA, a master regulator of the Caulobacter cell cycle. Proc. Natl. Acad.
1048 Sci. U. S. A. *99*, 4632–4637.
1049

1050 Lee, I., and Suzuki, C.K. (2008). Functional mechanics of the ATP-dependent Lon
1051 protease- lessons from endogenous protein and synthetic peptide substrates. Biochim
1052 Biophys Acta Proteins Proteom *1784*, 727–735.
1053
1054 Levchenko, I., Seidel, M., Sauer, R.T., and Baker, T.A. (2000). A Specificity-Enhancing
1055 Factor for the ClpXP Degradation Machine. Science *289*, 2354–2356.
1056
1057 Li, H., and Durbin, R. (2009). Fast and accurate short read alignment with Burrows-
1058 Wheeler transform. Bioinformatics *25*, 1754–1760.
1059
1060 Li, H., Handsaker, B., Wysoker, A., Fennell, T., Ruan, J., Homer, N., Marth, G.,
1061 Abecasis, G., and Durbin, R. (2009). The Sequence Alignment/Map format and
1062 SAMtools. Bioinformatics *25*, 2078–2079.
1063
1064 Liu, J., Francis, L.I., Jonas, K., Laub, M.T., and Chien, P. (2016). ClpAP is an auxiliary
1065 protease for DnaA degradation in Caulobacter crescentus. Mol. Microbiol. *102*, 1075–
1066 1085.
1067
1068 Lopez, K.E., Rizo, A.N., Tse, E., Lin, J.B., Scull, N.W., Thwin, A.C., Lucius, A.L.,
1069 Shorter, J., and Southworth, D.R. (2020). Conformational plasticity of the ClpAP AAA+
1070 protease couples protein unfolding and proteolysis. Nat. Struct. Mol. Biol. *27*, 406–416.
1071
1072 Mahmoud, S.A., and Chien, P. (2018). Regulated Proteolysis in Bacteria. Annu. Rev.
1073 Biochem. *87*, 677–696.
1074
1075 Martin, A., Baker, T.A., and Sauer, R.T. (2008). Protein unfolding by a AAA+ protease is
1076 dependent on ATP-hydrolysis rates and substrate energy landscapes.
1077 Nat. Struct. Mol. Biol. *15*, 139–145.

1078 Martin, A., Baker, T.A., and Sauer, R.T. (2008). Diverse pore loops of the AAA+ clpX
1079 machine mediate unassisted and adaptor-dependent recognition of ssrA-tagged
1080 substrates. Mol. cell *29*, 441–450.

1081 Mizusawa, S., and Gottesman, S. (1983). Protein degradation in Escherichia coli: the
1082 lon gene controls the stability of sulA protein. Proc. Natl. Acad. Sci. U. S. A. *80*, 358–
1083 362.
1084
1085 Persat, A., Stone, H.A., and Gitai, Z. (2014). The curved shape of caulobacter
1086 crescentus enhances surface colonization in flow. Nat. Commun. *5*, 1–9.
1087
1088 Quinlan, A.R., and Hall, I.M. (2010). BEDTools: a flexible suite of utilities for comparing
1089 genomic features. Bioinformatics *26*, 841–842.
1090
1091 Quon, K.C., Marczynski, G.T., and Shapiro, L. (1996). Cell cycle control by an essential
1092 bacterial two-component signal transduction protein. Cell *84*, 83–93.
1093

1094 R Core Team (2019). R: A language and Environment for Statistical Computing (R
1095 Foundation for Statistical Computing).
1096
1097 Ripstein, Z.A., Vahidi, S., Houry, W.A., Rubinstein, J.L., and Kay, L.E. (2020). A
1098 processive rotary mechanism couples substrate unfolding and proteolysis in the ClpXP
1099 degradation machinery. ELife *9*.
1100
1101 Robinson, M.D., McCarthy, D.J., and Smyth, G.K. (2009). edgeR: A Bioconductor
1102 package for differential expression analysis of digital gene expression data.
1103 Bioinformatics *26*, 139–140.

1104 Rogers, A., Townsley, L., Gallego-hernandez, A.L., Beyhan, S., Kwuan, L., and Yildiz,
1105 F.H. (2016). The LonA Protease Regulates Biofilm Formation, Motility, Virulence, and
1106 the Type VI Secretion System in Vibrio cholerae. J Bacteriol. *198*, 973–985.
1107
1108 Sauer, R.T., and Baker, T.A. (2011). AAA+ Proteases: ATP-Fueled Machines of Protein
1109 Destruction. Annu. Rev. Biochem *80*, 587–612.
1110
1111 Schneider, C.A., Rasband, W.S., and Eliceiri, K.W. (2012). NIH Image to ImageJ: 25
1112 years of image analysis. Nat. Methods *9*, 671–675.
1113
1114 Shin, M., Puchades, C., Asmita, A., Puri, N., Adjei, E., Luke Wiseman, R., Wali Karzai,
1115 A., and Lander, G.C. (2020). Structural basis for distinct operational modes and
1116 protease activation in AAA+ protease Lon. Sci Adv. *6*.
1117
1118 Skerker, J.M., Prasol, M.S., Perchuk, B.S., Biondi, E.G., and Laub, M.T. (2005). Two-
1119 component signal transduction pathways regulating growth and cell cycle progression in
1120 a bacterium: A system-level analysis. PLoS Biol. *3*.
1121
1122 Smith, S.C., Joshi, K.K., Zik, J.J., Trinh, K., Kamajaya, A., Chien, P., and Ryan, K.R.
1123 (2014). Cell cycle-dependent adaptor complex for ClpXP-mediated proteolysis directly
1124 integrates phosphorylation and second messenger signals. Proc. Natl. Acad. Sci. U. S.
1125 A. *111*, 14229–14234.
1126
1127 Tan, H.M., Kozdon, J.B., Shen, X., Shapiro, L., and McAdams, H.H. (2010). An
1128 essential transcription factor, SciP, enhances robustness of Caulobacter cell cycle
1129 regulation. Proc. Natl. Acad. Sci. U. S. A. *107*, 18985–18990.
1130
1131 Wang, J.D., Herman, C., Tipton, K.A., Gross, C.A., and Weissman, J.S. (2002).
1132 Directed evolution of substrate-optimized GroEL/S chaperonins. Cell *111*, 1027–1039.
1133
1134 Wang, K.H., Sauer, R.T., and Baker, T.A. (2007). ClpS modulates but is not essential
1135 for bacterial N-end rule degradation. Genes Dev. *21*, 403–408.
1136
1137 Witkin, E.M. (1946). Inherited Differences in Sensitivity to Radiation in Escherichia Coli.
1138 Proc. Natl. Acad. Sci. U. S. A. *32*, 59–68.
1139

1140 Wortinger, M., Sackett, M.J., and Brun, Y. V. (2000). CtrA mediates a DNA replication
1141 checkpoint that prevents cell division in Caulobacter crescentus. EMBO J. *19*, 4503–
1142 4512.
1143
1144 Wright, R., Stephens, C., Zweiger, G., Shapiro, L., and Alley, M.R.K. (1996).
1145 Caulobacter Lon protease has a critical role in cell-cycle control of DNA methylation.
1146 Genes Dev. *10*, 1532–1542.
1147
1148 Wu, D., Lim, E., Vaillant, F., Asselin-Labat, M.L., Visvader, J.E., and Smyth, G.K.
1149 (2010). ROAST: Rotation gene set tests for complex microarray experiments.
1150 Bioinformatics *26*, 2176–2182.
1151
1152 Yakhnin, A. V., Vinokurov, L.M., Surin, A.K., and Alakhov, Y.B. (1998). Green
1153 fluorescent protein purification by organic extraction. Protein Expr. Purif. *14*, 382–386.
1154
1155 Ye, X., Lin, J., Mayne, L., Shorter, J., and Walter Englander, S. (2020). Structural and
1156 kinetic basis for the regulation and potentiation of Hsp104 function. Proc. Natl. Acad.
1157 Sci. U. S. A. *117*, 9384-9392.
1158
1159 Yokom, A.L., Gates, S.N., Jackrel, M.E., Mack, K.L., Su, M., Shorter, J., and
1160 Southworth, D.R. (2016). Spiral architecture of the Hsp104 disaggregase reveals the
1161 basis for polypeptide translocation. Nat. Struct. Mol. Biol. *23*, 830–837.
1162
1163 Zeinert, R.D., Liu, J., Yang, Q., Du, Y., Haynes, C.M., and Chien, P. (2018). A legacy
1164 role for DNA binding of Lon protects against genotoxic stress. BioRxiv.
1165

Figure 1

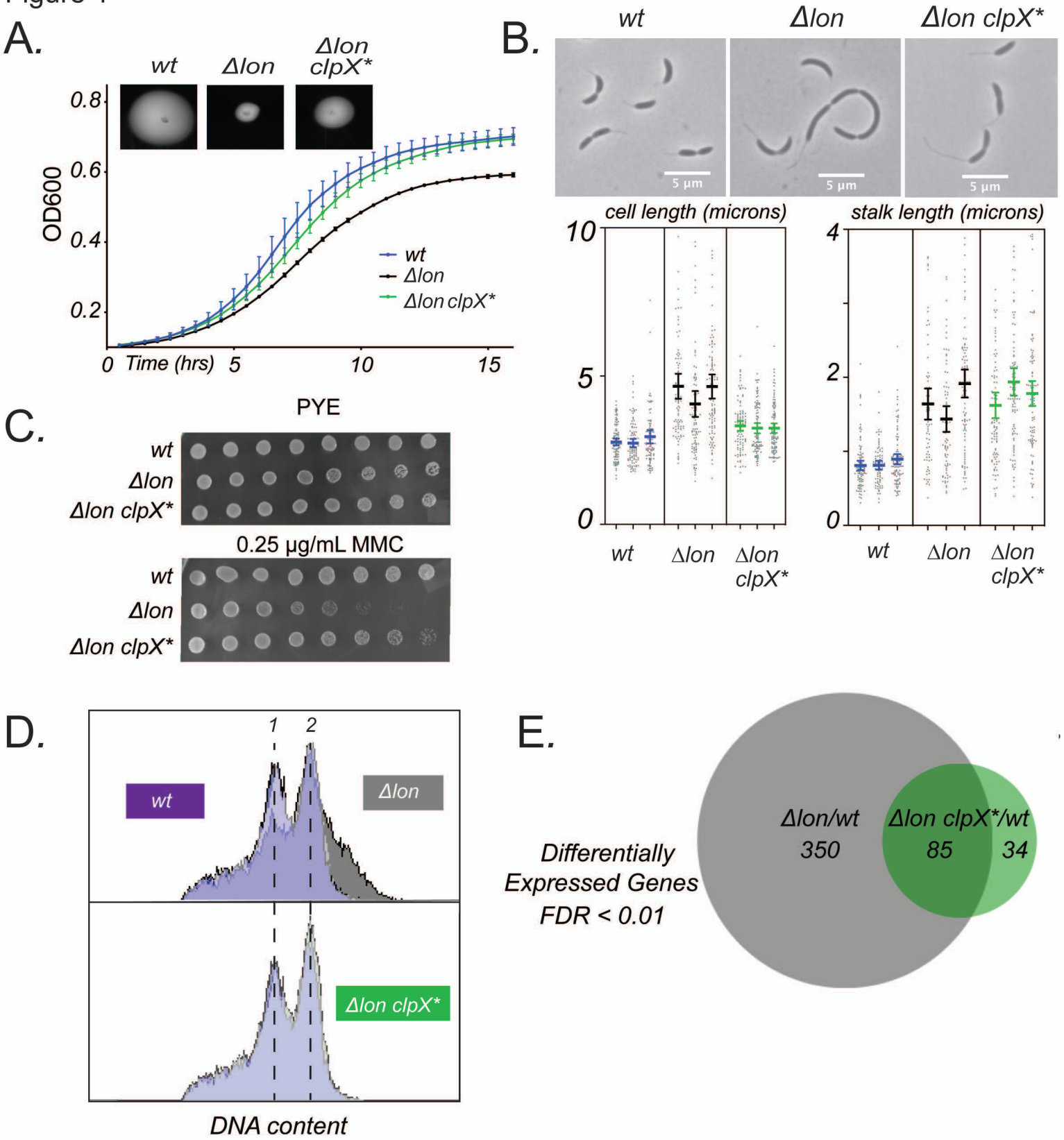
A.
wt
Δlon
Δlon clpX*
OD600
0.8
0.6
0.4
0.2
0
Time (hrs)
5
10
15
wt
Δlon
Δlon clpX*
B.
wt
Δlon
Δlon clpX*
5 µm
cell length (microns)
stalk length (microns)
10
5
0
4
2
0
wt
Δlon
Δlon clpX*
C.
PYE
wt
Δlon
Δlon clpX*
0.25 µg/mL MMC
wt
Δlon
Δlon clpX*
D.
1
2
wt
Δlon
Δlon clpX*
DNA content
E.
Differentially Expressed Genes FDR < 0.01
Δlon/wt
350
Δlon clpX*/wt
85
34

Figure 2

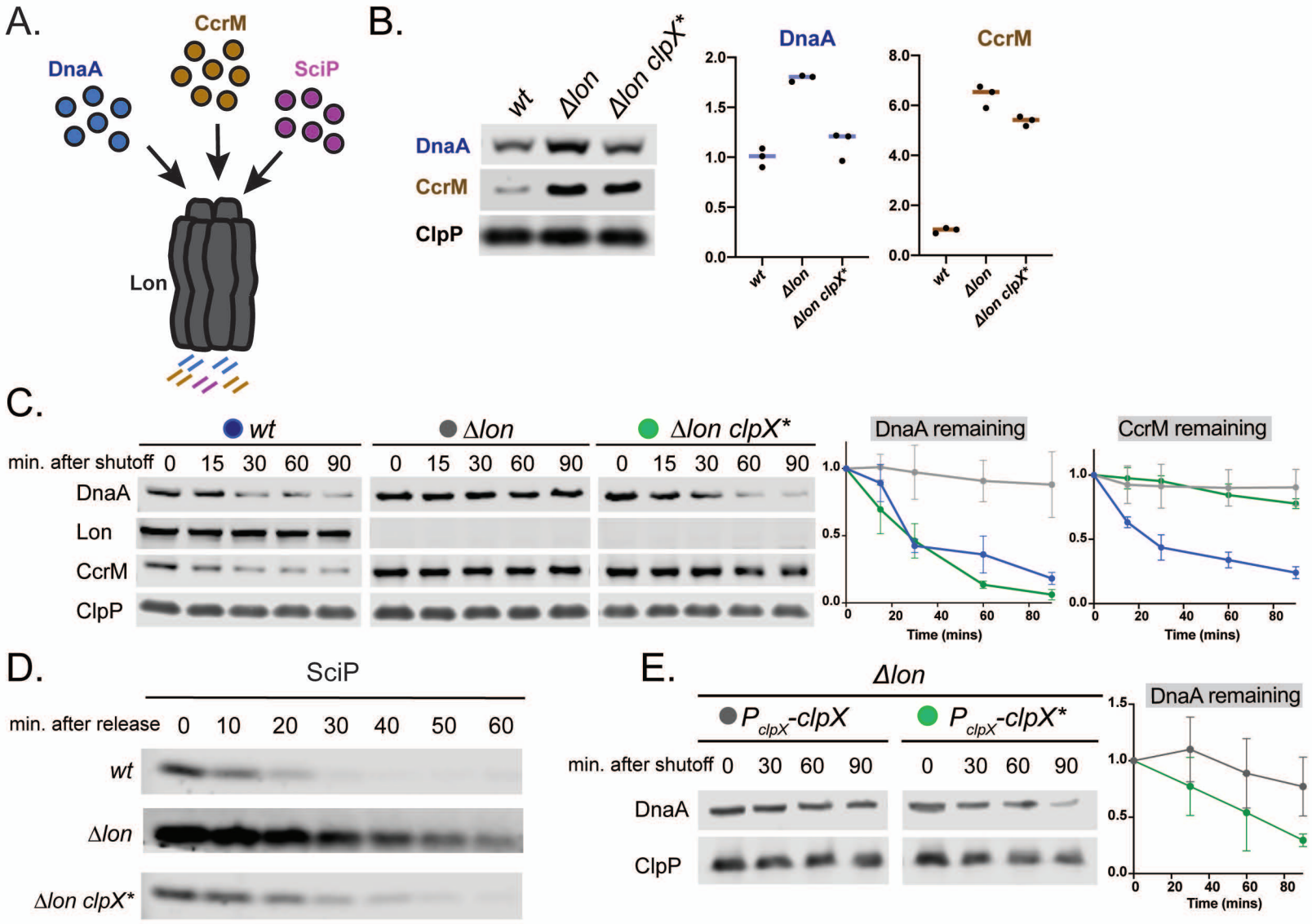
A.
CcrM
DnaA
SciP
Lon
B.
wt
Δlon
Δlon clpX*
DnaA
CcrM
ClpP
DnaA
CcrM
wt
Δlon
Δlon clpX*
C.
wt
Δlon
Δlon clpX*
min. after shutoff 0 15 30 60 90
DnaA
Lon
CcrM
ClpP
DnaA remaining
CcrM remaining
Time (mins)
D.
SciP
min. after release 0 10 20 30 40 50 60
wt
Δlon
Δlon clpX*
E.
Δlon
P clpX-clpX
P clpX-clpX*
min. after shutoff 0 30 60 90
DnaA
ClpP
DnaA remaining
Time (mins)

Figure 3

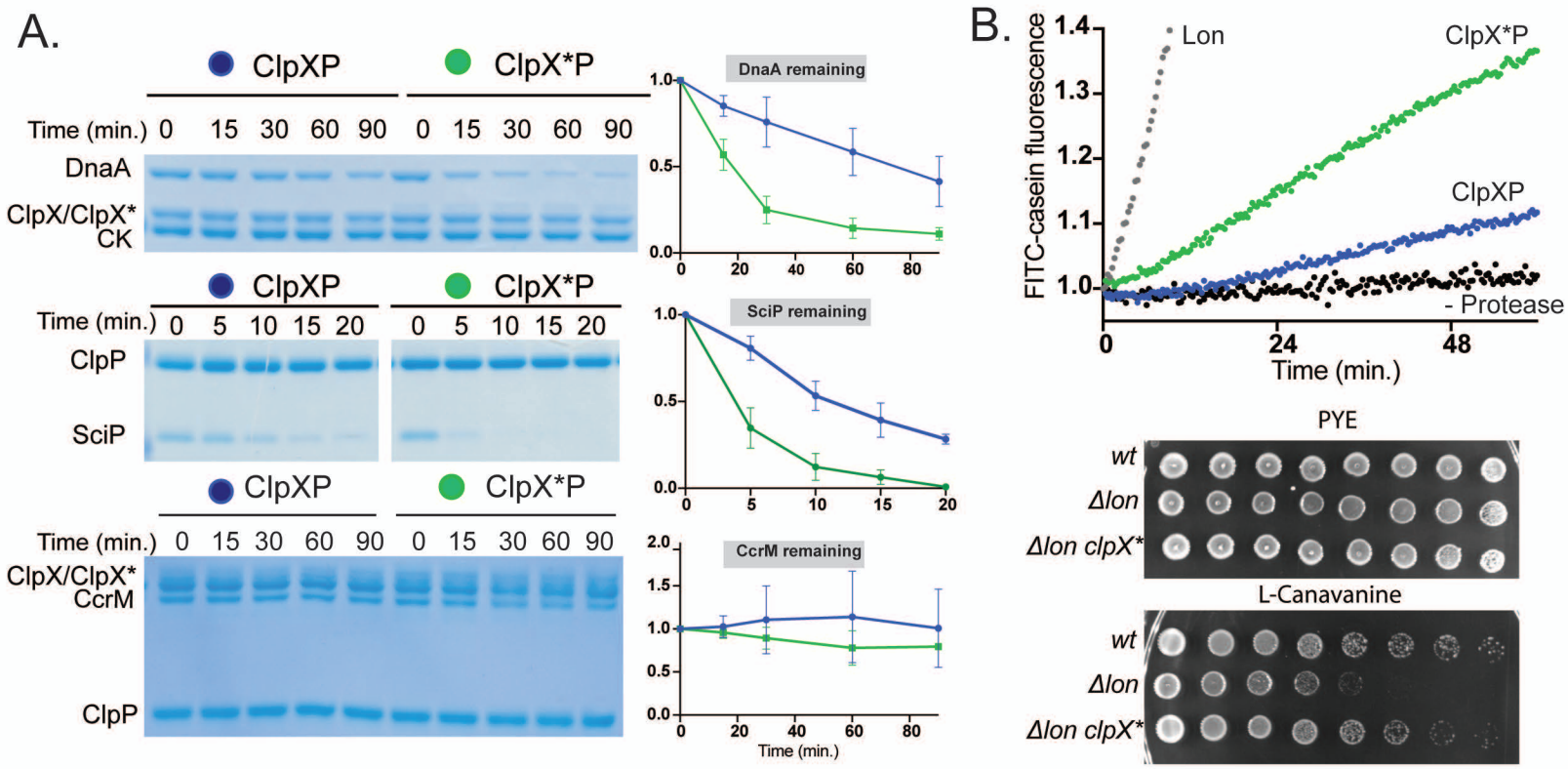
A.
ClpXP
ClpX*P
Time (min.) 0 15 30 60 90 0 15 30 60 90
DnaA
ClpX/ClpX*
CK
DnaA remaining
Time (min.) 0 5 10 15 20 0 5 10 15 20
ClpP
SciP
SciP remaining
Time (min.) 0 15 30 60 90 0 15 30 60 90
ClpX/ClpX*
CcrM
ClpP
CcrM remaining
Time (min.)
B.
FITC-casein fluorescence
Lon
ClpX*P
ClpXP
- Protease
Time (min.)
PYE
wt
Δlon
Δlon clpX*
L-Canavanine
wt
Δlon
Δlon clpX*

Figure 4

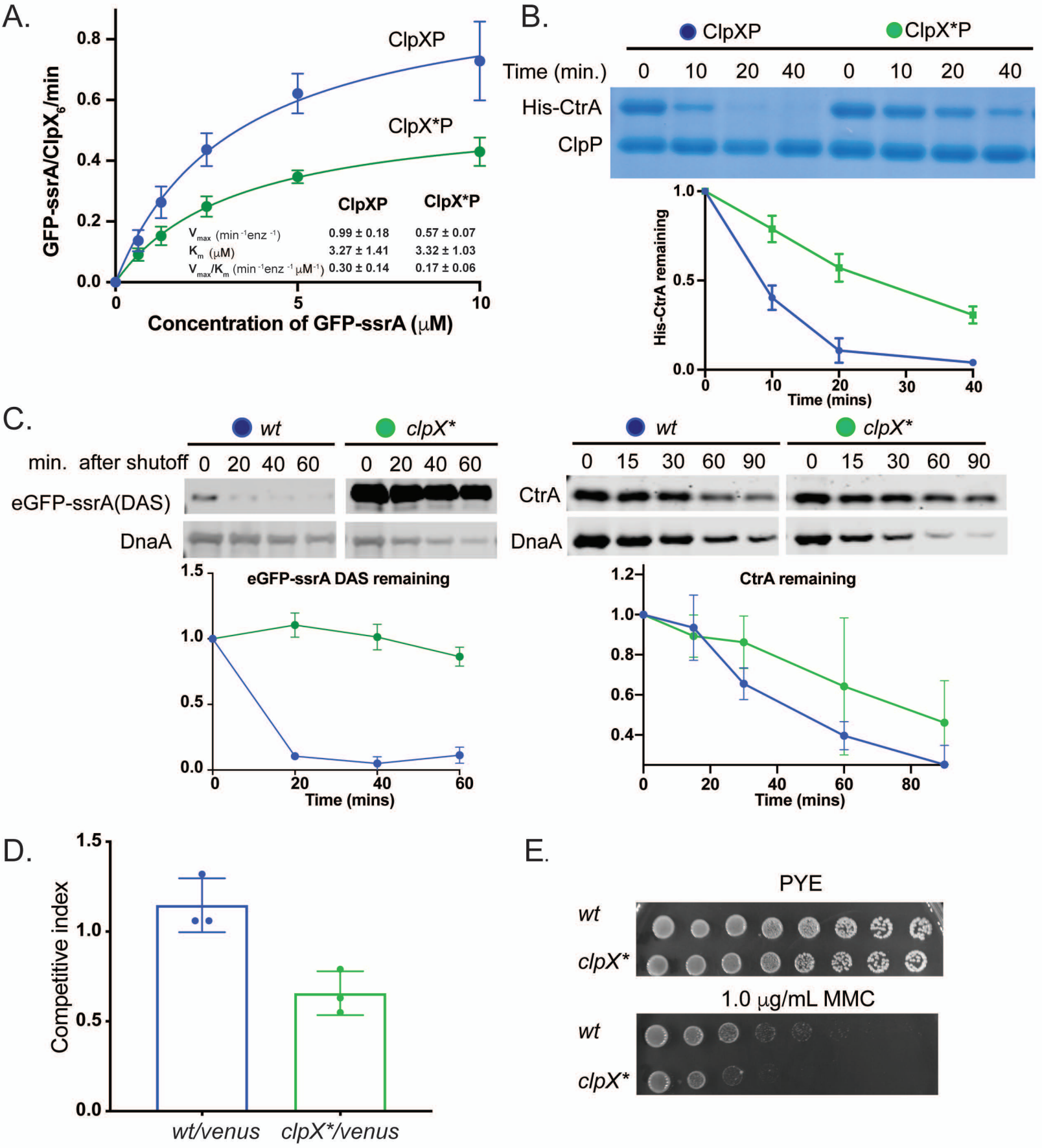
A.
ClpXP
ClpX*P
GFP-ssrA/ClpX6/min
Concentration of GFP-ssrA (μM)
ClpXP ClpX*P
Vmax (min-1enz-1) 0.99 ± 0.18 0.57 ± 0.07
Km (μM) 3.27 ± 1.41 3.32 ± 1.03
Vmax/Km (min-1enz-1μM-1) 0.30 ± 0.14 0.17 ± 0.06
B.
ClpXP
ClpX*P
Time (min.) 0 10 20 40 0 10 20 40
His-CtrA
ClpP
His-CtrA remaining
Time (mins)
C.
wt
clpX*
min. after shutoff 0 20 40 60 0 20 40 60
eGFP-ssrA(DAS)
DnaA
eGFP-ssrA DAS remaining
Time (mins)
wt
clpX*
0 15 30 60 90 0 15 30 60 90
CtrA
DnaA
CtrA remaining
Time (mins)
D.
Competitive index
wt/venus
clpX*/venus
E.
PYE
wt
clpX*
1.0 μg/mL MMC
wt
clpX*

Figure 5

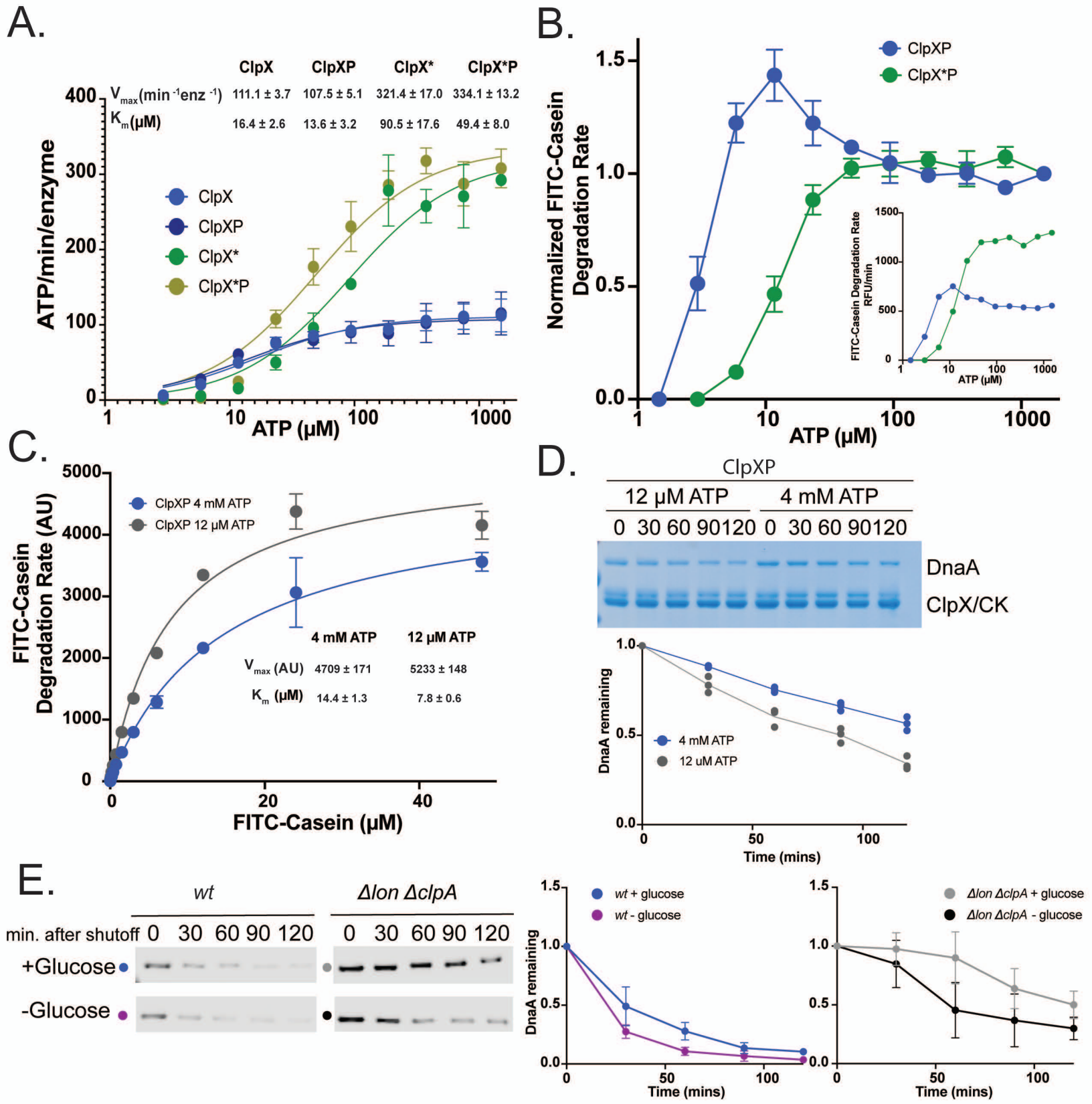
A.
ClpX ClpXP ClpX* ClpX*P
Vmax(min-1enz-1) 111.1 ± 3.7 107.5 ± 5.1 321.4 ± 17.0 334.1 ± 13.2
Km(μM) 16.4 ± 2.6 13.6 ± 3.2 90.5 ± 17.6 49.4 ± 8.0
ATP/min/enzyme
ClpX
ClpXP
ClpX*
ClpX*P
ATP (μM)
B.
Normalized FITC-Casein Degradation Rate
ClpXP
ClpX*P
FITC-Casein Degradation Rate RFU/min
ATP (μM)
C.
FITC-Casein Degradation Rate (AU)
ClpXP 4 mM ATP
ClpXP 12 μM ATP
4 mM ATP 12 μM ATP
Vmax (AU) 4709 ± 171 5233 ± 148
Km (μM) 14.4 ± 1.3 7.8 ± 0.6
FITC-Casein (μM)
D.
ClpXP
12 μM ATP 4 mM ATP
0 30 60 90 120 0 30 60 90 120
DnaA
ClpX/CK
DnaA remaining
4 mM ATP
12 uM ATP
Time (mins)
E.
wt Δlon ΔclpA
min. after shutoff 0 30 60 90 120 0 30 60 90 120
+Glucose
-Glucose
DnaA remaining
wt + glucose
wt - glucose
Time (mins)
Δlon ΔclpA + glucose
Δlon ΔclpA - glucose
Time (mins)

Figure 6

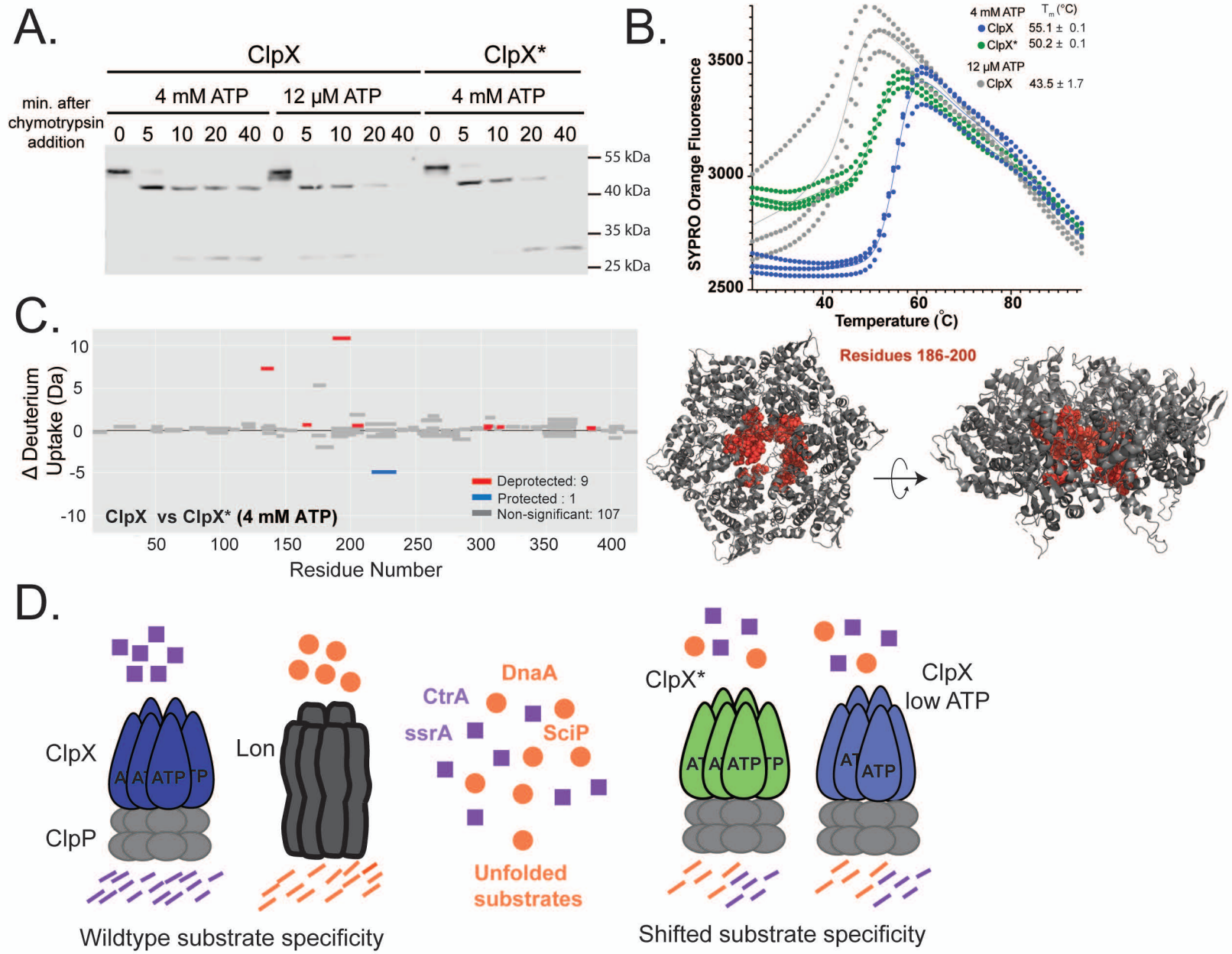
A.
ClpX
ClpX*
4 mM ATP
12 μM ATP
4 mM ATP
min. after chymotrypsin addition
0 5 10 20 40 0 5 10 20 40 0 5 10 20 40
55 kDa
40 kDa
35 kDa
25 kDa
B.
4 mM ATP
T_m (°C)
ClpX 55.1 ± 0.1
ClpX* 50.2 ± 0.1
12 μM ATP
ClpX 43.5 ± 1.7
SYPRO Orange Fluorescnce
3500
3000
2500
40
60
80
Temperature (°C)
C.
Δ Deuterium Uptake (Da)
10
5
0
-5
-10
ClpX vs ClpX* (4 mM ATP)
Deprotected: 9
Protected : 1
Non-significant: 107
50
100
150
200
250
300
350
400
Residue Number
Residues 186-200
D.
ClpX
ClpP
Lon
CtrA
ssrA
DnaA
SciP
Unfolded substrates
ClpX*
ClpX low ATP
Wildtype substrate specificity
Shifted substrate specificity